H. Ishibuchi, R. Imada, Y. Setoguchi and Y. Nojima, "Hypervolume subset selection for triangular and inverted triangular Pareto fronts of three-objective problems," Proc. of The 14th ACM/SIGEVO Workshop on Foundations of Genetic Algorithms (in press)

Hypervolume Subset Selection for Triangular and Inverted Triangular Pareto Fronts of Three-Objective Problems

Hisao Ishibuchi, Ryo Imada, Yu Setoguchi, and Yusuke Nojima
Department of Computer Science and Intelligent Systems
Osaka Prefecture University
Sakai, Osaka, 599-8531
Japan
{hisaoi@, ryo.imada@ci., yu.setoguchi@ci., nojima@}cs.osakafu-u.ac.jp

ABSTRACT

Hypervolume subset selection is to find a pre-specified number of solutions for hypervolume maximization. The optimal distribution of solutions on the Pareto front has been theoretically studied for two-objective problems in the literature. In this paper, we discuss hypervolume subset selection for three-objective problems with triangular and inverted triangular Pareto fronts. Our contribution is to show that the effect of the location of a reference point for hypervolume calculation on the optimal distribution of solutions is totally different between triangular and inverted triangular Pareto fronts. When the reference point is far from the Pareto front, most solutions are on the sides of the inverted triangular Pareto front while they are evenly distributed over the entire triangular Pareto front. These properties seem to hold in multiobjective problems with four or more objectives. We also show that the effect of the location of a reference point on the optimal distribution is totally different between maximization and minimization problems with the same triangular Pareto fronts. This property is supported by the fact that maximization problems with triangular Pareto fronts are equivalent to minimization problems with inverted triangular Pareto fronts. The optimal distribution of solutions is also discussed when the reference point is close to the Pareto front (i.e., when its location is between the nadir point and the Pareto front).

CCS Concepts

•**Computing methodologies; Optimization algorithms; Search methodologies**.

Keywords

Evolutionary multiobjective optimization; Pareto front; solution subset selection; hypervolume maximization.

1. INTRODUCTION

Hypervolume [23] has been frequently used to evaluate a set of solutions in the evolutionary multiobjective optimization (EMO) community [24] (i.e., to compare the search ability of different EMO algorithms). This is mainly because the hypervolume is a Pareto compliant performance indicator (e.g., see [22]). It has also been frequently used in indicator-based algorithms such as SMS-EMOA [5] and HypE [3] where multiobjective optimization is handled as single-objective hypervolume maximization. In those algorithms, a population of solutions is evolved to maximize its hypervolume. Hypervolume maximization needs the convergence of solutions to the Pareto front as well as their diversification over the entire Pareto front. When a two-objective problem has a linear Pareto front, the optimal distribution of solutions for hypervolume maximization is equidistant solutions on the Pareto front [1], [9].

Recently, hypervolume maximization by selecting a pre-specified number of solutions from a large number of candidates has been actively studied in the EMO community [4], [6], [7], [11]-[13], [15], [17], [20]. This task is referred to as hypervolume subset selection. The optimal distribution of solutions for hypervolume maximization has been also theoretically studied in the literature [1], [2], [9], [10], [21]. Almost all of those studies are for two-objective problems. Whereas the optimal distribution of solutions for multiobjective problems with three or more objectives was discussed in [21], a single-dimensional curve was assumed as the Pareto front. In this paper, we discuss hypervolume maximization for multiobjective problems with three or more objectives. We focus on a frequently-used many-objective test problem DTLZ1 [8] and its two variants: inverted DTLZ1 [19] and Max-DTLZ1 [18]. We show that these three problems have different optimal distributions for hypervolume maximization while they have the same (or inverted) Pareto front in the normalized objective space.

In Figure 1, we show solution sets obtained for the three-objective DTLZ1 and inverted DTLZ1 problems by SMS-EMOA [5]. A population of size 50 was evolved for 1,000,000 generations to maximize the hypervolume for the reference point (20, 20, 20). Since the Pareto front of each test problem is included in the cube $[0.0, 0.5]^3$, the reference point (20, 20, 20) is far from the Pareto front. In this paper, we explain why all solutions in Figure 1 (b) are on the sides of the inverted triangular Pareto front whereas well-distributed solutions are obtained over the entire triangular Pareto front in Figure 1 (a).

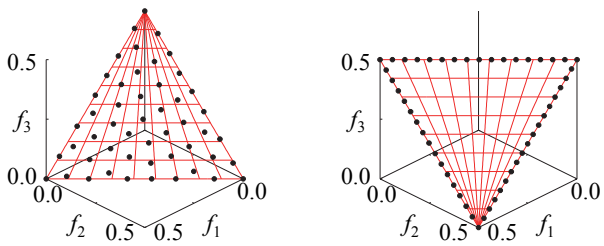

(a) DTLZ1. (b) Inverted DTLZ1.

Figure 1. Obtained solution sets by SMS-EMOA when the reference point is far from the Pareto front: (20, 20, 20).

FOGA'17, January 12-15, 2017, Copenhagen, Denmark.

DOI: http://dx.doi.org/10.1145/12345.67890

The triangular Pareto front of the three-objective DTLZ1 problem is written as follows [8]:

$$PF = \{(f_1, f_2, f_3) \mid f_1 + f_2 + f_3 = 0.5,\ 0 \le f_i \le 0.5 \text{ for } i = 1, 2, 3\}. \quad (1)$$

Thus the nadir point is (0.5, 0.5, 0.5). The three-objective inverted DTLZ1 problem [19] has the same nadir point since its inverted triangular Pareto front is written as follows:

$$PF = \{(f_1, f_2, f_3) \mid f_1 + f_2 + f_3 = 1,\ 0 \le f_i \le 0.5 \text{ for } i = 1, 2, 3\}. \quad (2)$$

In the same manner as in Figure 1, we applied SMS-EMOA to DTLZ1 and its inverted version using the nadir point (0.5, 0.5, 0.5) as the reference point. Figure 2 shows the obtained solution set for each test problem. Whereas the two solution sets in Figure 2 are well distributed over the Pareto fronts, they have a clear difference. No solutions are very close to the sides of the inverted triangular Pareto front in Figure 2 (b) whereas about six solutions in Figure 2 (a) are very close to each side of the triangular Pareto front. In this paper, we explain the reason for this difference.

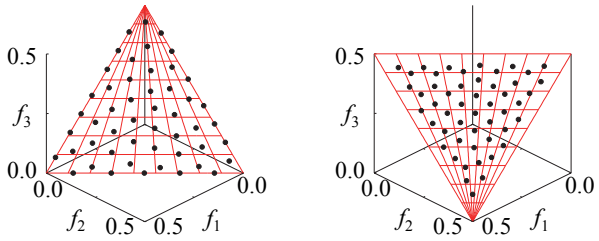

(a) DTLZ1. (b) Inverted DTLZ1.

Figure 2. Obtained solution sets by SMS-EMOA when the nadir point (0.5, 0.5, 0.5) is used as the reference point.

For comparison, we also examine another variant of DTLZ1 called Max-DTLZ1 [18]. In Max-DTLZ1, all objectives to be minimized in DTLZ1 are maximized. In this paper, we handle DTLZ1, inverted DTLZ1 and Max-DTLZ1 under a special setting where the number of distance variables is always 0 while the number of position variables is $m-1$ for m-objective problems. In this setting, all feasible solutions of each problem are Pareto optimal. As a result, the DTLZ1 and Max-DTLZ1 problems have the same triangular Pareto front in (1). It should be noted that the ideal point (0, 0, 0) of DTLZ1 is the nadir point of Max-DTLZ1.

In the same manner as in Figure 1 and Figure 2, we applied SMS-EMOA to Max-DTLZ1 using the nadir point (0, 0, 0) as the reference point. We also applied SMS-EMOA to Max-DTLZ1 using (–20, –20, –20) as the reference point. This reference point is far from the Pareto front. The obtained solution set for each reference point is shown in Figure 3.

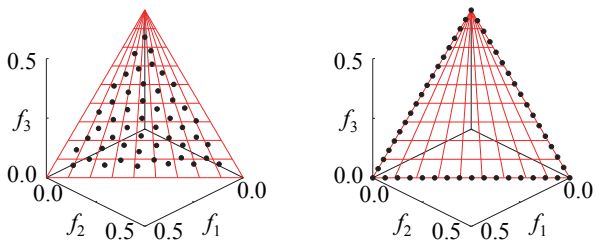

(a) Nadir point (0, 0, 0). (b) (–20, –20, –20).

Figure 3. Obtained solution sets by SMS-EMOA for Max-DTLZ1 for the reference points (0, 0, 0) and (–20, –20, –20).

From Figures 1-3, we can see that the obtained solution sets for Max-DTLZ1 in Figure 3 are similar to those for the inverted DTLZ1 in Figures 1 and 2. This is because Max-DTLZ1, which is a maximization problem with a triangular Pareto front (see Figure 3), is equivalent to a minimization problem with an inverted triangular Pareto front as we will explain later in this paper.

This paper is organized as follows. In Section 2, first we briefly explain basic concepts in multiobjective optimization such as Pareto optimality, Pareto front, hypervolume, and hypervolume subset selection. Then we explain the Pareto front of each test problem: DTLZ1, inverted DTLZ1 and Max-DTLZ1. We show that the three test problems have exactly the same Pareto front:

$$PF = \{(f_1, f_2, f_3) \mid f_1 + f_2 + f_3 = 1,\ 0 \le f_i \le 1 \text{ for } i = 1, 2, 3\}, \quad (3)$$

in the normalized objective space when the inverted DTLZ1 is handled as the equivalent maximization problem. When the inverted DTLZ1 is handled as a minimization problem in the normalized objective space, its Pareto front can be written as $PF = \{(f_1, f_2, f_3) \mid f_1 + f_2 + f_3 = 2,\ 0 \le f_i \le 1 \text{ for } i = 1, 2, 3\}$. In Section 3, we discuss hypervolume subset selection for the case where the reference point is far from the Pareto front. We explain why totally different distributions of solutions are obtained in Figure 1 for the three-objective DTLZ1 and inverted DTLZ1 problems. In Section 4, we discuss hypervolume subset selection for the case where the nadir point is used as the reference point. We explain why different solution sets are obtained in Figure 2 for the three-objective DTLZ1 and inverted DTLZ1 problems. We also discuss the optimal distribution of solutions when a reference point is close to the Pareto front (i.e., when its location is between the nadir point and the Pareto front). In this case, different solution sets are obtained by SMS-EMOA for DTLZ1 and Max-DTLZ1 as shown in Figure 4. We explain why obtained solutions for DTLZ1 are in an inverted triangle whereas those for Max-DTLZ1 are triangular. In Section 5, we discuss the effect of the reference point on the hypervolume-based comparison results of different solution sets. Experimental results on other test problems are shown in Section 6. Finally we conclude this paper in Section 7.

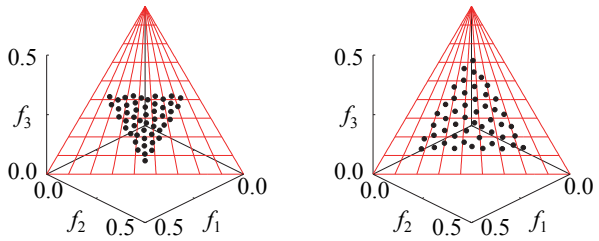

(a) DTLZ1. (b) Max-DTLZ1.

Figure 4. Obtained solution sets by SMS-EMOA when the reference point is close to the Pareto front, which is specified as (0.25, 0.25, 0.25) in (a) and (0.05, 0.05, 0.05) in (b).

2. MULTIOBJECTIVE TEST PROBLEMS

2.1 Multiobjective Optimization

First we show some basic concepts in multiobjective optimization before explaining hypervolume subset selection and test problems. Let us assume that we have an m-objective minimization problem:

$$\text{Minimize } f_1(\boldsymbol{x}), f_2(\boldsymbol{x}), \ldots, f_m(\boldsymbol{x}) \text{ subject to } \boldsymbol{x} \in \boldsymbol{X}, \quad (4)$$

where $\boldsymbol{x}$ is a decision vector, $\boldsymbol{X}$ is its feasible region, and $f_i(\boldsymbol{x})$ is the ith objective to be minimized ($i = 1, 2, \ldots, m$). The m-objective

minimization problem in (4) can be rewritten as the following m-objective maximization problem by multiplying each objective by (−1):

$$\text{Maximize } -f_1(\boldsymbol{x}), -f_2(\boldsymbol{x}), ..., -f_m(\boldsymbol{x}) \text{ subject to } \boldsymbol{x} \in \boldsymbol{X}. \quad (5)$$

Let us assume that $\boldsymbol{a}$ and $\boldsymbol{b}$ are two solutions in the objective space of the m-objective minimization problem in (4): $\boldsymbol{a} = (a_1, a_2, ..., a_m)$ and $\boldsymbol{b} = (b_1, b_2, ..., b_m)$. When the following condition holds, $\boldsymbol{b}$ is referred to as being dominated by $\boldsymbol{a}$ (i.e., $\boldsymbol{a}$ is better than $\boldsymbol{b}$ in the sense of Pareto dominance): $a_i \le b_i$ for all i's and $a_j < b_j$ for at least one j. This condition can be rewritten as $\boldsymbol{a} \le \boldsymbol{b}$ (i.e., $a_i \le b_i$ for all i's) and $\mathbf{a} \ne \boldsymbol{b}$. When a solution $\boldsymbol{x}^*$ (i.e., a point $\boldsymbol{f}(\boldsymbol{x}^*) = (f_1(\boldsymbol{x}^*), f_2(\boldsymbol{x}^*), ..., f_m(\boldsymbol{x}^*))$ in the objective space) is not dominated by any other solution, $\boldsymbol{x}^*$ is referred to as a Pareto optimal solution. In general, a multiobjective optimization problem has a number of Pareto optimal solutions. The set of all Pareto optimal solutions is the Pareto optimal solution set. The Pareto optimal solution set in the objective space is referred to as the Pareto front. The Pareto front shows the tradeoff relation among the objectives.

A multiobjective problem has two special points in the objective space. One is the ideal point z_{Ideal}, which is defined by the best value of each objective. The other is the nadir point z_{Nadir}, which is defined by the worst value of each objective in the Pareto optimal solution set. These two points are illustrated in Figure 5 for minimization and maximization problems.

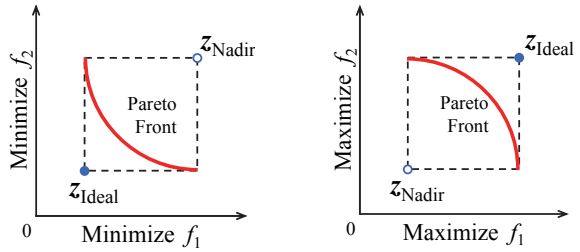

(a) Minimization problem. (b) Maximization problem.

Figure 5. Ideal point and nadir point for minimization and maximization problems.

2.2 Hypervolume Subset Selection

A reference point for hypervolume calculation is a point in the m-dimensional objective space. We denote the reference point by $\boldsymbol{r} = (r_1, r_2, ..., r_m)$. The hypervolume of a point $\boldsymbol{a} = (a_1, a_2, ..., a_m)$ is the area ($m = 2$), volume ($m = 3$) or hypervolume ($m \ge 4$) of the dominated region by $\boldsymbol{a}$ bounded by the reference point $\boldsymbol{r}$. This region can be written for the m-objective minimization problem as follows (see Figure 6 (a)):

$$D(\boldsymbol{a}, \boldsymbol{r}) = \{(z_1, z_2, ..., z_m) \mid a_i \le z_i \le r_i \text{ for } i = 1, 2, ..., m\}. \quad (6)$$

The hypervolume of a set of μ points, $S = \{\boldsymbol{a}^1, \boldsymbol{a}^2, ..., \boldsymbol{a}^\mu\}$, is the area, volume or hypervolume of the union of the dominated region by each point (see Figure 6 (b)):

$$D(S, \boldsymbol{r}) = D(\boldsymbol{a}^1, \boldsymbol{r}) \cup D(\boldsymbol{a}^2, \boldsymbol{r}) \cup \ ... \ \cup D(\boldsymbol{a}^\mu, \boldsymbol{r}). \quad (7)$$

If the reference point $\boldsymbol{r}$ is not dominated by any point in the point set S, the hypervolume of S is 0. This is because the dominated region by each point bounded by the reference point is empty.

For the m-objective maximization problem, the hypervolume of a single point $\boldsymbol{a}$ is calculated from the following dominated region by $\boldsymbol{a}$ bounded by the reference point $\boldsymbol{r}$ (see Figure 7 (a)):

$$D(\boldsymbol{a}, \boldsymbol{r}) = \{(z_1, z_2, ..., z_m) \mid r_i \le z_i \le a_i \text{ for } i = 1, 2, ..., m\}. \quad (8)$$

The hypervolume of a set of μ points, $S = \{\boldsymbol{a}^1, \boldsymbol{a}^2, ..., \boldsymbol{a}^\mu\}$, is calculated in the same manner as in (7). That is, the hypervolume is the area, volume or hypervolume of the union of the dominated region by each point (see Figure 7 (b)).

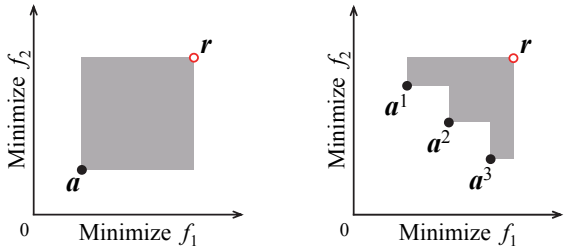

(a) Dominated region by $\boldsymbol{a}$. (b) Dominated region by S.

Figure 6. Illustration of the hypervolume of a point $\boldsymbol{a}$ in (a) and the hypervolume of a point set $\boldsymbol{S} = \{\boldsymbol{a}^1, \boldsymbol{a}^2, \boldsymbol{a}^3\}$ in (b) for minimization problems.

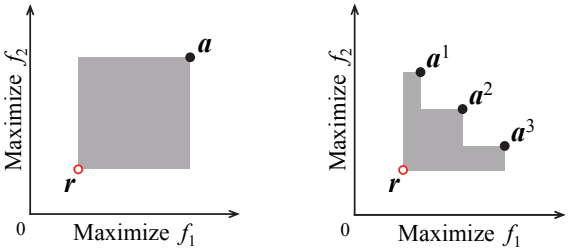

(a) Dominated region by $\boldsymbol{a}$. (b) Dominated region by S.

Figure 7. Illustration of the hypervolume of a point $\boldsymbol{a}$ in (a) and the hypervolume of a point set $\boldsymbol{S} = \{\boldsymbol{a}^1, \boldsymbol{a}^2, \boldsymbol{a}^3\}$ in (b) for maximization problems.

The hypervolume contribution of a point $\boldsymbol{a}^j$ in a point set S ($\boldsymbol{a}^j \in S$) is the amount of decrease in the hypervolume by removing $\boldsymbol{a}^j$ from S. That is, the hypervolume contribution of $\boldsymbol{a}^j$ in S is defined as $HV(S) - HV(S \backslash \{\boldsymbol{a}^j\})$ where $HV(S)$ is the hypervolume of S and $HV(S \backslash \{\boldsymbol{a}^j\})$ is the hypervolume of S excluding $\boldsymbol{a}^j$. Figure 8 shows the hypervolume contribution of $\boldsymbol{a}^2$ in the point set $S = \{\boldsymbol{a}^1, \boldsymbol{a}^2, \boldsymbol{a}^3\}$.

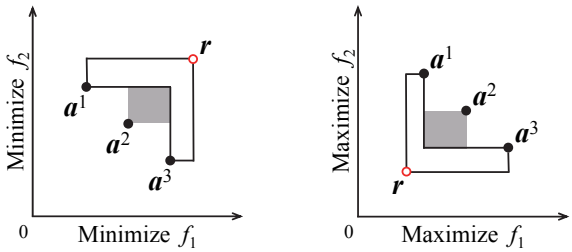

(a) Minimization problem. (b) Maximization problem.

Figure 8. Hypervolume contribution of $\boldsymbol{a}^2$ in $\boldsymbol{S} = \{\boldsymbol{a}^1, \boldsymbol{a}^2, \boldsymbol{a}^3\}$.

Hypervolume subset selection for finding μ solutions can be written as the following optimization problem:

$$\text{Maximize } HV(S) \text{ subject to } |S| = \mu. \quad (9)$$

Hypervolume subset selection is usually formulated as a discrete optimization problem for selecting μ solutions from a number of given non-dominated solutions (i.e., from a pre-specified set of

candidate solutions). In this paper, we discuss the selection of μ solutions for hypervolume maximization from all Pareto optimal solutions. That is, the entire Pareto optimal solution set is assumed as the candidate solution set in our hypervolume subset selection.

The optimal μ-distribution is the distribution of μ solutions which maximizes the hypervolume, i.e., the distribution of μ solutions in the optimal solution set S^* of the hypervolume subset selection problem in (9). When the Pareto front of a two-objective problem is linear (i.e., a line), it was shown in the literature (e.g., see [2]) that the hypervolume is maximized by a set of equidistant points on the Pareto front as shown in Figure 9. The two extreme solutions of the Pareto front are included in the optimal solution set S^* when some conditions on the Pareto front and the location of the reference point are satisfied (for details, see [2]).

The optimal solution set S^* (i.e., the optimal μ-distribution) does not depend on the location of the reference point in Figure 9 as long as the following two conditions hold: (i) the two extreme solutions of the Pareto front are included in the optimal solution set S^*, and (ii) the reference point $\boldsymbol{r}$ is dominated by the nadir point as in Figure 9. The second condition (ii) holds when the reference point is far from the Pareto front (see Figure 9). Under these conditions, subset selection is to maximize the hypervolume of $(\mu-2)$ solutions in the shaded region in Figure 10 (since the two extreme solutions are included in the optimal solution set S^*).

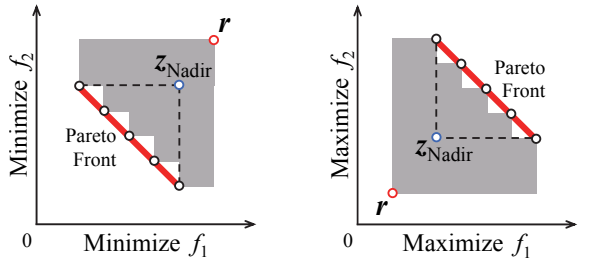

(a) Minimization problem. (b) Maximization problem.

Figure 9. Optimal solution set S^* with five solutions.

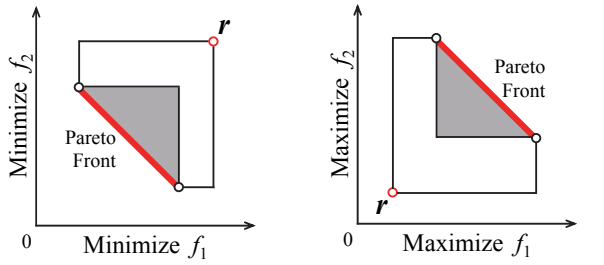

(a) Minimization problem. (b) Maximization problem.

Figure 10. Hypervolume contribution of all solutions on the Pareto front excluding the two extreme solutions.

2.3 DTLZ1 Test Problem

As a scalable test problem where the number of objectives can be arbitrarily specified, DTLZ1 [8] has been frequently used for evaluating the search ability of many-objective evolutionary algorithms. Each objective in DTLZ1 can be written as

$$\text{Minimize} \quad f_i(\boldsymbol{x}) = (1+g(\boldsymbol{x}_{\text{dis}}))h_i(\boldsymbol{x}_{\text{pos}}), \ i=1, 2, ..., m, \qquad (10)$$

where the decision vector $\boldsymbol{x} = (x_1, x_2, \ldots, x_{m+k-1})$ is separable into the first $m-1$ position variables in $\boldsymbol{x}_{\text{pos}} = (x_1, x_2, \ldots, x_{m-1})$ and the other k distance variables in $\boldsymbol{x}_{\text{dis}} = (x_m, x_{m+1}, \ldots, x_{m+k-1})$. The number of decision variables is specified by the parameter k. In (10), $h_i(\boldsymbol{x}_{\text{pos}})$ determines the shape of the Pareto front ($h_i(\boldsymbol{x}_{\text{pos}}) \geq 0$) while $g(\boldsymbol{x}_{\text{dis}})$ specifies the distance from the Pareto front ($g(\boldsymbol{x}_{\text{dis}}) \geq 0$). All decision variables have the same constraint condition: $0 \leq x_j \leq 1$ for $j = 1, 2, ..., m+k-1$.

The Pareto optimal solution set of DTLZ1 is the set of all feasible solutions with $g(\boldsymbol{x}_{\text{dis}}) = 0$. DTLZ1 has no Pareto optimal solution with $g(\boldsymbol{x}_{\text{dis}}) > 0$. Since the decision vector $\boldsymbol{x}$ is separable into $\boldsymbol{x}_{\text{pos}}$ and $\boldsymbol{x}_{\text{dis}}$, the Pareto front of DTLZ1 can be written as

$$f_i(\boldsymbol{x}) = h_i(\boldsymbol{x}_{\text{pos}}), \ i=1, 2, ..., m, \qquad (11)$$

where $0 \leq x_j \leq 1$ for $j = 1, 2, ..., m-1$. It is well known that DTLZ1 has the following linear Pareto front [8]:

$$\{(f_1, f_2, ..., f_m) \mid \sum_{i=1}^{m} f_i = 0.5, \ 0 \leq f_i \leq 0.5 \text{ for } i = 1, 2, ..., m\}. \qquad (12)$$

When we applied SMS-EMOA to DTLZ1 in Section 1, we specified the number of distance variables in $\boldsymbol{x}_{\text{dis}}$ as zero (i.e., $k = 0$) to remove $g(\boldsymbol{x}_{\text{dis}})$ from each objective in (10). Under this setting, all feasible solutions of DTLZ1 are Pareto optimal. This means that SMS-EMOA examined only Pareto optimal solutions in Section 1. We also applied SMS-EMOA to the inverted DTLZ1 and Max-DTLZ1 problems in the same setting (i.e., $k = 0$) in Section 1. This is to focus on hypervolume subset selection from Pareto optimal solutions.

2.4 Variants of DTLZ Test Problems

The inverted DTLZ1 problem was formulated in [19] as a scalable test problem with an inverted triangular Pareto front by modifying each objective function of DTLZ1 as

$$u_i(\boldsymbol{x}) = 0.5(1+g(\boldsymbol{x}_{\text{dis}})) - f_i(\boldsymbol{x}), \ i = 1, 2, ..., m, \qquad (13)$$

where $u_i(\boldsymbol{x})$ is the ith objective of the inverted DTLZ1 problem. As in DTLZ1, the Pareto optimal solution set of the inverted DTLZ1 problem is the set of all feasible solutions with $g(\boldsymbol{x}_{\text{dis}}) = 0$. Using $g(\boldsymbol{x}_{\text{dis}}) = 0$ in the right-hand side of (13) and also in (10), the Pareto front of the inverted DTLZ1 problem can be written as

$$u_i(\boldsymbol{x}) = 0.5 - h_i(\boldsymbol{x}_{\text{pos}}), \ i=1, 2, ..., m. \qquad (14)$$

Since the Pareto front in (12) is generated by $h_i(\boldsymbol{x}_{\text{pos}})$ in (11) using all feasible solutions in $\boldsymbol{x}_{\text{pos}}$, we have the following relation for $u_i(\boldsymbol{x})$ on the Pareto front in (14) from (11) and (12):

$$\sum_{i=1}^{m} u_i(\boldsymbol{x}) = \sum_{i=1}^{m} 0.5 - \sum_{i=1}^{m} h_i(\boldsymbol{x}_{\text{pos}}) = 0.5m - 0.5 = (m-1)/2, \qquad (15)$$

where $0 \leq u_i(\boldsymbol{x}) \leq 0.5$ ($i = 1, 2, ..., m$). Since all feasible solutions satisfying (15) are Pareto optimal, the Pareto front of the m-objective inverted DTLZ1 is written as

$$\{(f_1, f_2, ..., f_m) \mid \sum_{i=1}^{m} f_i = (m-1)/2, \ 0 \leq f_i \leq 0.5 \text{ for } i=1, 2, ..., m\}. \qquad (16)$$

Max-DTLZ1 was formulated in [18] by replacing "Minimize" with "Maximize" in the formulation of DTLZ1 as

$$\text{Maximize} \quad f_i(\boldsymbol{x}) = (1+g(\boldsymbol{x}_{\text{dis}}))h_i(\boldsymbol{x}_{\text{pos}}), \ i=1, 2, ..., m. \qquad (17)$$

Except for this replacement, Max-DTLZ1 is the same as DTLZ1. Thus these two test problems have the same objective functions, the same decision variables, and the same feasible region.

In general, DTLZ1 and Max-DTLZ1 have different Pareto fronts [18]. However, when $k = 0$ (i.e., the number of distance variables is 0), Max-DTLZ1 has the same linear Pareto front as DTLZ1. That is, the Pareto front of Max-DTLZ1 can be also written by (12). This is because the entire feasible region of DTLZ1, which is the same as the entire feasible region of Max-DTLZ1, is the Pareto front of DTLZ1 when $k = 0$ (i.e., because no feasible solution is dominated by any other feasible solutions when $k = 0$).

For simplicity of explanations, we normalize the objective space of DTLZ1 and Max-DTLZ1 so that the Pareto front in (12) is normalized in $[0, 1]^m$ as follows (i.e., $[0, 0.5]^m \rightarrow [0, 1]^m$):

$$\{(f_1, f_2, ..., f_m) \mid \sum_{i=1}^{m} f_i = 1,\ 0 \le f_i \le 1 \text{ for } i = 1, 2, ..., m\}. \quad (18)$$

We also apply the same normalization to the objective space of the inverted DTLZ1 so that the Pareto front in (16) is normalized in $[0, 1]^m$ as follows (i.e., $[0, 0.5]^m \rightarrow [0, 1]^m$):

$$\{(f_1, f_2, ..., f_m) \mid \sum_{i=1}^{m} f_i = (m-1),\ 0 \le f_i \le 1 \text{ for } i = 1, 2, ..., m\}. \quad (19)$$

Let us explain that the normalized Pareto front in (19) of the inverted DTLZ1 problem can be viewed as being the same as the normalized Pareto front in (18) of Max-DTLZ1. In general, the minimization problem of $f_i(\boldsymbol{x})$ is equivalent to the maximization problem of $-f_i(\boldsymbol{x})$. So, we can formulate the following equivalent maximization problem of $q_i(\boldsymbol{x})$ from the inverted DTLZ1 problem with $f_i(\boldsymbol{x})$, $i = 1, 2, ..., m$:

$$\text{Maximize } q_i(\boldsymbol{x}) = -f_i(\boldsymbol{x}),\ i = 1, 2, ..., m. \quad (20)$$

By replacing $f_i(\boldsymbol{x})$ with $-q_i(\boldsymbol{x})$ in (19), we obtain the following Pareto front of the maximization problem in (20):

$$\{(q_1, q_2, ..., q_m) \mid \sum_{i=1}^{m} q_i = (1-m),\ -1 \le q_i \le 0 \text{ for } i = 1, 2, ..., m\}. \quad (21)$$

We normalize the objective space of the maximization problem in (20) so that the Pareto front in (21) is normalized in $[0, 1]^m$ as follows (i.e., $[-1, 0]^m \rightarrow [0, 1]^m$: $q_i = f_i - 1$ in (21)):

$$\{(f_1, f_2, ..., f_m) \mid \sum_{i=1}^{m} f_i = 1,\ 0 \le f_i \le 1 \text{ for } i = 1, 2, ..., m\}. \quad (22)$$

This is the same as the normalized Pareto front of Max-DTLZ1 in (18). That is, the normalized inverted triangular Pareto front in (19) of the inverted DTLZ1 problem is equivalent to the normalized triangular Pareto front in (18) of Max-DTLZ1.

In general (i.e., when $k > 0$), the Pareto front of Max-DTLZ1 can be written as

$$\{(f_1, f_2, ..., f_m) \mid \sum_{i=1}^{m} f_i = g_{\max},\ 0 \le f_i \le g_{\max} \text{ for } i = 1, 2, ..., m\}, \quad (23)$$

where $g_{\max}$ is the maximum value of the distance function $g(\boldsymbol{x}_{\text{dis}})$. This Pareto front can be normalized to $[0, 1]^m$. Thus we can see that Max-DTLZ1 and DTLZ1 have the same normalized Pareto front, which is also the same as the normalized Pareto front of the inverted DTLZ1 when it is handled as a maximization problem.

Since the inverted triangular Pareto front of the inverted DTLZ1 problem is equivalent to the triangular Pareto front of Max-DTLZ1, we mainly discuss the optimal distribution of solutions on the normalized triangular Pareto front in (22) for minimization and maximization problems in the rest of this paper.

3. FAR REFERENCE POINT

In this section, we discuss the optimal distribution of solutions on the normalized triangular Pareto front in (22) when the reference point for hypervolume calculation is far from the Pareto front. Our main focus in this section is the effect of the location of the reference point on the optimal distribution of solutions.

As we explained in Section 2, the location of the reference point has no effect on the optimal distribution of solutions for two-objective problems under the following conditions: (i) the two extreme solutions of the Pareto front are included in the optimal solution set, and (ii) the reference point is dominated by the nadir point. When these conditions hold, the location of the reference point has no effects on the hypervolume contribution of each solution except for the two extreme solutions as shown in Figure 9 and Figure 10. In this section, we discuss whether the three extreme solutions of the triangular Pareto front of a three-objective problem play the same role as in the case of two objectives. Then we show that the extreme solutions of the triangular Pareto front play different roles between the DTLZ1 problem and the Max-DTLZ1 problem (i.e., between DTLZ1 and the inverted DTLZ1). We will see from our discussions that the extreme solutions of the triangular Pareto front of only DTLZ1 play the same role as those of two-objective problems.

3.1 DTLZ1

The normalized triangular Pareto front of the three-objective DTLZ1 problem is shown by the shaded triangle in Figure 11, which is written as $f_1 + f_2 + f_3 = 1$ and $0 \le f_i \le 1$ for $i = 1, 2, 3$. In Figure 11, the nadir point is (1, 1, 1) since DTLZ1 is a minimization problem. We assume that the reference point $\boldsymbol{r} = (r_1, r_2, r_3)$ is far from the Pareto front (e.g., $\boldsymbol{r} = (10, 10, 10)$). We also assume that the three extreme solutions A (1, 0, 0), B (0, 1, 0), C (0, 0, 1) of the normalized triangular Pareto front in Figure 11 are included in the optimal solution set S^*.

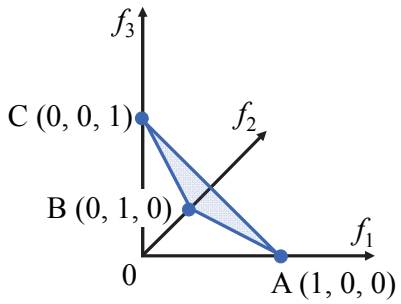

Figure 11. The normalized triangular Pareto front of DTLZ1: $f_1 + f_2 + f_3 = 1$ and $0 \le f_i \le 1$ for $i = 1, 2, 3$.

The dominated region by each extreme solution in Figure 11 bounded by the reference point $\boldsymbol{r} = (r_1, r_2, r_3)$ can be written as

$$D(\text{A}, \boldsymbol{r}) = \{(z_1, z_2, z_3) \mid 1 \le z_1 \le r_1, 0 \le z_2 \le r_2, 0 \le z_3 \le r_3\}, \quad (24)$$

$$D(\text{B}, \boldsymbol{r}) = \{(z_1, z_2, z_3) \mid 0 \le z_1 \le r_1, 1 \le z_2 \le r_2, 0 \le z_3 \le r_3\}, \quad (25)$$

$$D(\text{C}, \boldsymbol{r}) = \{(z_1, z_2, z_3) \mid 0 \le z_1 \le r_1, 0 \le z_2 \le r_2, 1 \le z_3 \le r_3\}. \quad (26)$$

Figure 12 shows the dominated region by the extreme solution A bounded by the reference point $\boldsymbol{r}$. We can see from Figure 12 that all solutions in the cuboid $[1, r_1] \times [0, r_2] \times [0, r_3]$ (i.e., all solutions with $1 \le f_1$) are dominated by the extreme solution A. In the same manner as Figure 12, we can show that all solutions in the cuboid

$[0, r_1] \times [1, r_2] \times [0, r_3]$ (i.e., all solutions with $1 \le f_2$) are dominated by the extreme solution B. We can also show that all solutions in the cuboid $[0, r_1] \times [0, r_2] \times [1, r_3]$ (i.e., all solutions with $1 \le f_3$) are dominated by the extreme solution C.

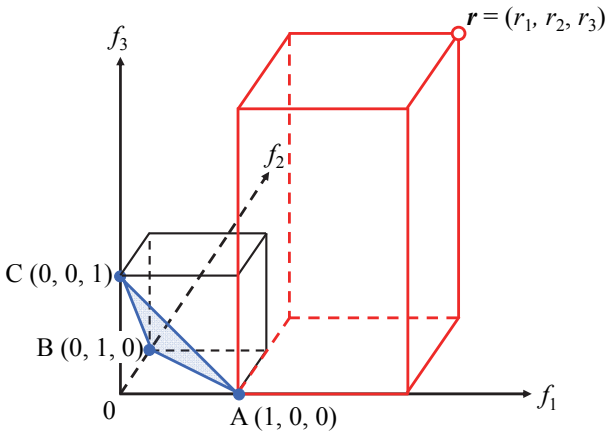

Figure 12. The dominated region by the extreme solution A.

From these discussions, we can see that the dominated region by the triangular Pareto front in the three-dimensional objective space is also dominated by at least one of the three extreme solutions A, B and C except for the inside of the unit cube $[0, 1]^3$ in Figure 12. This situation is the same as the case of two-objective problems in Figure 10. The optimal distribution of solutions except for the three extreme solutions can be specified by maximizing their hypervolume inside the unit cube $[0, 1]^3$. As a result, when the reference point is far from the Pareto front, the location of the reference point has no effect on the optimal distribution of solutions as long as the three extreme solutions are included in the optimal solution set. Thus a set of well-distributed solutions was obtained by SMS-EMOA in Figure 1 (a) when (20, 20, 20) was used as the reference point.

These discussions can be easily extended to the case of four or more objectives. Let us assume that an m-objective minimization problem has the normalized triangular Pareto front defined by (22): $f_1 + f_2 + \ldots + f_m = 1$ and $0 \le f_i \le 1$. This Pareto front has the m extreme solutions: (1, 0, 0, ..., 0), (0, 1, 0, ..., 0), ..., (0, 0, ..., 0, 1). The dominated region by the first extreme solution A bounded by the reference point $\boldsymbol{r} = (r_1, r_2, \ldots, r_m)$ can be written as

$$D(\mathrm{A}, \boldsymbol{r}) = \{(z_1, \ldots, z_m) \mid 1 \le z_1 \le r_1, 0 \le z_i \le r_i \text{ for } i = 2, \ldots, m\}. \quad (27)$$

That is, all solutions in the hyper-cuboid $[1, r_1] \times [0, r_2] \times [0, r_3] \times \ldots \times [0, r_m]$ are dominated by A. Since the dominated region by each extreme solution can be written in the same manner, we can see that the dominated region by the triangular Pareto front in the m-dimensional objective space is also dominated by at least one of the m extreme solutions except for the inside of the unit hypercube $[0, 1]^m$. This means that the location of the reference point has no effect on the optimal distribution as long as (i) all the m extreme solutions are included in the optimal solution set and (ii) the reference point is far from the Pareto front.

These discussions show that the extreme solutions of the triangular Pareto front of the multiobjective DTLZ1 problem with three or more objectives play the same role in hypervolume calculation as in the case of two-objective problems in Figure 10 when the reference point is far from the Pareto front.

The above-mentioned role of the extreme solutions of the Pareto front in hypervolume calculation can be explained in a different manner using the projection from the three-dimensional objective space to a two-dimensional subspace. Let us assume that a solution set S has the following four solutions L (0, 0.5, 0.5), M (0.5, 0, 0.5), N (0.5, 0.5, 0) and Z (1/3, 1/3, 1/3) on the Pareto front in addition to the three extreme solutions A, B and C in Figure 12. Their projections to the two-dimensional subspace with f_2 and f_3 are shown in Figure 13 (a). Since DTLZ1 is a minimization problem, the extreme solution A dominates all the other solutions in the two-dimensional subspace with f_2 and f_3 in Figure 13 (a). That is, the f_2-f_3 subspace in Figure 13 (a) has only a single non-dominated solution.

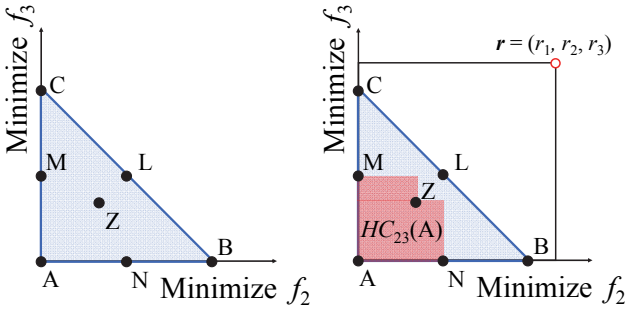

(a) Seven solutions. (b) Hypervolume contribution.

Figure 13. Projection of the Pareto front and the seven solutions to the two-dimensional subspace with f_2 and f_3.

When the extreme solution A is included in a solution set S, no other solution has a positive hypervolume contribution in the f_2-f_3 subspace in Figure 13 (a). Let us denote the hypervolume contribution of A in the f_2-f_3 subspace as HC_{23}(A), which is shown by the red area in Figure 13 (b). When the reference point $\boldsymbol{r} = (r_1, r_2, r_3)$ is far from the Pareto front, the extreme solution A has a large hypervolume contribution calculated as $(r_1 - 1) \times HC_{23}(\mathrm{A})$ in the original three-dimensional objective space, which increases as the value of r_1 increases. Hypervolume contribution of no other solution increases as the value of r_1 increases. These discussions for the extreme solution A (1, 0, 0) on the f_2-f_3 subspace hold for the extreme solution B (0, 1, 0) on the f_1-f_3 subspace and the extreme solution C (0, 0, 1) on the f_1-f_2 subspace. Thus hypervolume contribution of any non-extreme solution in Figure 13 does not depend on the location of the reference point as far as the reference point is dominated by the nadir point.

These discussions can be generalized to the case of m objectives. Let us assume that a solution set S includes some Pareto optimal solutions and all the m extreme solutions (1, 0, ..., 0), (0, 1, 0, ..., 0), ..., (0, ..., 0, 1) of the triangular Pareto front defined by $f_1 + f_2 + \ldots + f_m = 1$ and $0 \le f_i \le 1$. First we consider the projection to the $(m-1)$-dimensional subspace with f_2, f_3, ..., f_m. The extreme solution (1, 0, ..., 0) is projected to (0, 0, ..., 0), which dominates all the other solutions in the f_2-f_3-...-f_m subspace. Thus the increase of r_1 of the reference point $\boldsymbol{r} = (r_1, r_2, \ldots, r_m)$ increases only the hypervolume contribution of the extreme solution (1, 0, ..., 0). The increase of r_1 has no effect on the hypervolume contribution of any other solution. These discussions hold for the other extreme solutions of the Pareto front and the other $(m-1)$-dimensional subspaces (e.g., for the extreme solution (0, 1, 0, ..., 0) and the f_1-f_3-...-f_m subspace). Thus the hypervolume contribution of any non-

extreme solution does not depend on the location of the reference point as far as (i) all the m extreme solutions of the Pareto front are included in the solution set, and (ii) the reference point is dominated by the nadir point.

These discussions show that the optimal distribution of solutions for hypervolume maximization does not depend on the location of a reference point when (i) all the m extreme solutions of the triangular Pareto front of the m-dimensional DTLZ1 problem are included in the optimal solution set and (ii) the reference point is far from the Pareto front.

3.2 Max-DTLZ1 and Inverted DTLZ1

In this subsection, we discuss the optimal distribution of solutions for hypervolume maximization for the Max-DTLZ1 problem and the inverted-DTLZ1 problem.

Let us consider a three-objective maximization problem with the normalized triangular Pareto front in Figure 11. As in Subsection 3.1, we assume that the three extreme solutions A (1, 0, 0), B (0, 1, 0) and C (0, 0, 1) of the normalized triangular Pareto front in Figure 11 are included in a solution set S for hypervolume maximization. We also assume that the reference point $\boldsymbol{r} = (r_1, r_2, r_3)$ is far from the Pareto front: $r_1 << 0$, $r_2 << 0$ and $r_3 << 0$.

In our maximization problem with the normalized triangular Pareto front, the dominated region by each extreme solution bounded by the reference point $\boldsymbol{r} = (r_1, r_2, r_3)$ can be written as

$$D(\mathrm{A}, \boldsymbol{r}) = \{(z_1, z_2, z_3) \mid r_1 \le z_1 \le 1, r_2 \le z_2 \le 0, r_3 \le z_3 \le 0\}, \quad (28)$$

$$D(\mathrm{B}, \boldsymbol{r}) = \{(z_1, z_2, z_3) \mid r_1 \le z_1 \le 0, r_2 \le z_2 \le 1, r_3 \le z_3 \le 0\}, \quad (29)$$

$$D(\mathrm{C}, \boldsymbol{r}) = \{(z_1, z_2, z_3) \mid r_1 \le z_1 \le 0, r_2 \le z_2 \le 0, r_3 \le z_3 \le 1\}. \quad (30)$$

Figure 14 (and Figure 15) shows the dominated region by the extreme solution A (and C) bounded by the reference point $\boldsymbol{r}$. From these figures, we can see that some regions outside the unit cube $[0, 1]^3$ are not dominated by any extreme solution whereas they are dominated by the Pareto front. For example, we can see from Figure 14 and Figure 15 that the triangle pole in Figure 16 in the region with $f_2 \le 0$ is not dominated by any extreme solution whereas it is dominated by the Pareto front.

The triangle pole in the region with $f_2 \le 0$ in Figure 16, which is dominated by the Pareto front but not dominated by any extreme solution, can be written as follows:

$$\{(z_1, z_2, z_3) \mid 0 \le z_1 \le 1, r_2 \le z_2 \le 0, 0 \le z_3 \le 1, z_1 + z_3 \le 1\}. \quad (31)$$

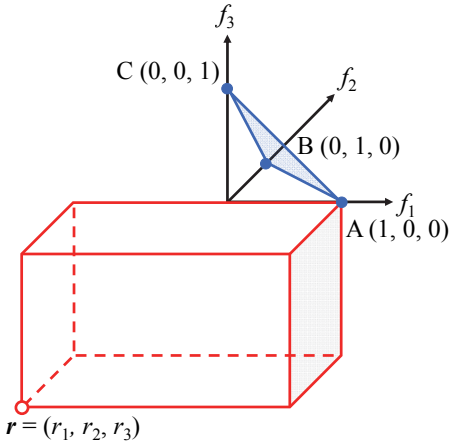

Figure 14. The dominated region by the extreme solution A.

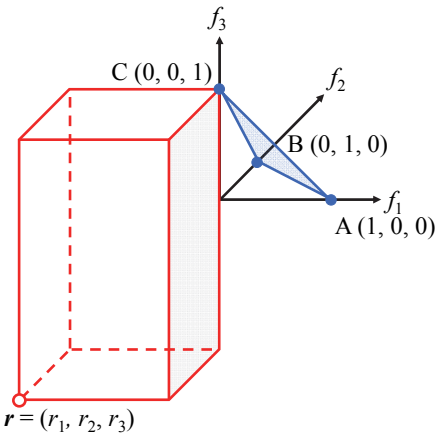

Figure 15. The dominated region by the extreme solution C.

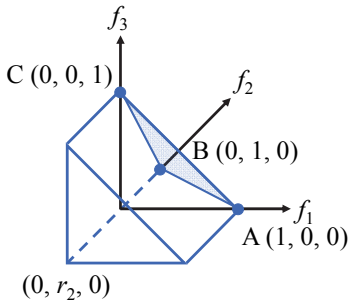

Figure 16. Uncovered region with $f_2 \le 0$ by the three extreme solutions A, B and C.

Similar triangle poles exist in the regions with $f_1 \le 0$ and $f_3 \le 0$. They can be written as

$$\{(z_1, z_2, z_3) \mid r_1 \le z_1 \le 0, 0 \le z_2 \le 1, 0 \le z_3 \le 1, z_2 + z_3 \le 1\}, \quad (32)$$

$$\{(z_1, z_2, z_3) \mid 0 \le z_1 \le 1, 0 \le z_2 \le 1, r_3 \le z_3 \le 0, z_1 + z_2 \le 1\}. \quad (33)$$

From (31)-(33) and Figure 16, we can see that the length of each uncovered triangle pole depends on the location of the reference point. The length increases (i.e., its hypervolume increases) by moving the reference point away from the Pareto front. Thus the hypervolume contributions of some non-extreme solutions depend on the location of the reference point. This means that the optimal distribution of solutions for hypervolume maximization also depends on its location.

Since all solutions are on the sides of the triangular Pareto front of the three-objective Max-DTLZ1 problem in Figure 3 (b) when the reference point is far from the Pareto front, one may expect that the hypervolume contribution of a solution on a side of the Pareto front of Max-DTLZ1 increases by moving the reference point away from the Pareto front. One may also expect that the hypervolume contribution of a solution inside the Pareto front does not increase by moving the reference point away from the Pareto front (since no solution exists inside the the triangular Pareto front in Figure 3 (b)). Let us examine these expectations.

In Figure 17, we show the hypervolume contribution of a solution M (0.5, 0, 0.5) in the solution set {A, B, C, M} where M is the midpoint of A and C. The hypervolume contribution of M is the volume of the following square pole (which is $|r_2|/4$):

$$\{(z_1, z_2, z_3) \mid 0 \le z_1 \le 0.5, r_2 \le z_2 \le 0, 0 \le z_3 \le 0.5\}. \quad (34)$$

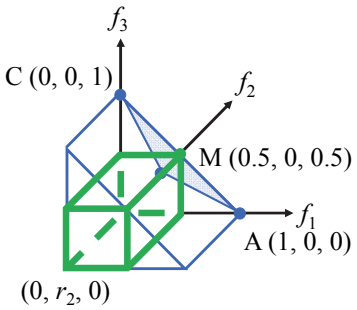

Figure 17. Hypervolume contribution of the solution M (0.5, 0, 0.5) in the solution set {A, B, C, M}.

The square pole dominated by M in Figure 17 covers 1/2 of the uncovered triangle pole with $f_2 \le 0$. In addition to M, let us include solutions L (0, 0.5, 0.5) and N (0.5, 0.5, 0) to the solution set {A, B, C, M}. The hypervolume contributions of L, M and N in {A, B, C, L, M, N} are $|r_1|/4|$, $|r_2|/4$ and $|r_3|/4$, respectively, which are calculated in different regions. In Figure 17, the volume of the square pole is the hypervolume contribution of M.

Now, let us consider the inclusion of a new solution Y (0.25, 0, 0.75) to the solution set {A, B, C, L, M, N} as shown in Figure 18. The hypervolume contribution of Y is the volume of the smaller square pole in Figure 18, which is calculated as $|r_2|/16$.

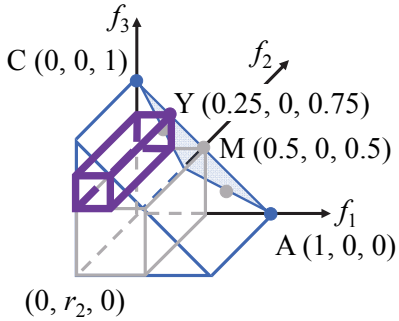

Figure 18. Hypervolume contribution of the solution Y (0.25, 0, 0.75) in the solution set {A, B, C, L, M, N}.

Instead of including the solution Y, let us consider the inclusion of a solution Z = (1/3, 1/3, 1/3), which is at the center of the triangular Pareto front. The hypervolume contribution of Z is calculated as 1/27 (i.e., the volume of the cube $[0, 1/3]^3$) since the outside of the cube $[0, 0.5]^3$ is covered by the solution set {A, B, C, L, M, N}. When the reference point is far from the Pareto front (i.e., $|r_2|$ is large), the hypervolume contribution 1/27 of the solution Z (1/3, 1/3, 1/3) at the center of the Pareto front is much smaller than $|r_2|/16$ of the solution Y (0.25, 0, 0.75) on the line AC. This may explain why all solutions are on the sides of the Pareto front in Figure 3 (b) for hypervolume maximization using 50 solutions for the reference point (–20, –20, –20).

Of course, the solution Z (1/3, 1/3, 1/3) at the center of the Pareto front has a large hypervolume contribution when only the three extreme solutions A, B and C are included in the solution set. That is, the hypervolume contribution of Z in the solution set {A, B, C, Z} is calculated as $|r_1|/9 + |r_2|/9 + |r_3|/9 + 1/27$. The first three terms are the volumes of the three square poles in the three regions with $f_1 \le 0$, $f_2 \le 0$ and $f_3 \le 0$. However, these three parts completely disappear by including the three solutions L, M and N.

It should be noted that the inclusion of Z decreases the hypervolume contribution of each of L, M and N from $|r_i|/4$ to $(|r_i|/4 - |r_i|/9)$, which is still large when $|r_i|$ is large. As shown by these calculations, it is difficult for inside solutions to continue to have a large hypervolume contribution.

Let us assume that all solutions in the solution set are on the sides of the triangular Pareto front. Under this assumption, we discuss the hypervolume maximization in the triangle pole in Figures 16-18 by a pre-specified number of solutions on the line AC. Since the contribution of each solution is always the volume of a pole of the length $|r_2|$, this task is exactly the same as the hypervolume maximization for a two-objective problem with the linear Pareto front between (1, 0) and (0, 1) for the reference point (0, 0). This may explain why equidistant solutions are obtained in Figure 3 (b).

It is difficult to extend these discussions on the three-objective Max-DTLZ1 problem to the case of four or more objectives. However, our experimental results suggest that all solutions are on the sides of the triangular Pareto front in the case of four objectives (i.e., four-objective Max-DTLZ1). In Figure 19, we show 50 solutions obtained after 1,000,000 generations of SMS-EMOA for the four-objective Max-DTLZ1 problem when the reference point is (–20, –20, –20, –20). The obtained solutions in the four-dimensional objective space are shown by projecting them to its two-dimensional subspaces. Figure 19 suggests that all solutions are on the sides of the triangular Pareto front of the four-objective Max-DTLZ1 problem.

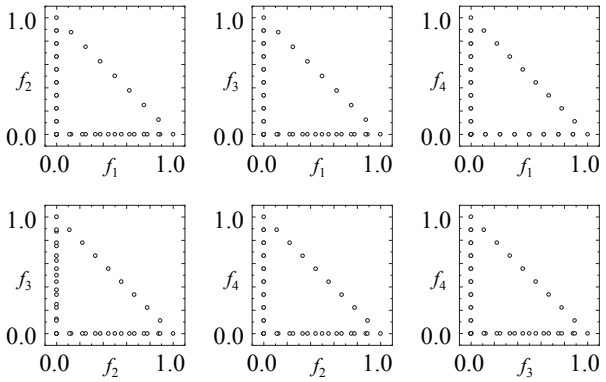

Figure 19. The obtained solutions for the four-objective Max-DTLZ1 problem for the reference point (–20, –20, –20, –20).

As in the previous subsection, let us discuss the effect of the location of the reference point on the optimal distribution of solutions using the projection of solutions of the three-objective Max-DTLZ1 problem to the two-dimensional subspace with f_2 and f_3. We use the solution set including the seven solutions A, B, C, L, M, N and Z in Figure 13 (see Figure 20).

Since our problem in this subsection is a maximization problem, all solutions on the side BC of the triangular Pareto front between solution B (0, 1, 0) and solution C (0, 0, 1) are Pareto optimal in the f_2-f_3 subspace (see Figure 20). In Figure 20, we show the hypervolume contribution of B, C and L on the side BC in the f_2-f_3 subspace. Not only the two extreme solutions B (0, 1, 0) and C (0, 0, 1) but also the solution L (0, 1/2, 1/2) on the side BC has a positive hypervolume contribution in the f_2-f_3 subspace. Thus their hypervolume contributions increase as the absolute value of r_1 increases (i.e., the value of r_1 decreases, e.g., to –20). Since these

discussions hold for the f_1-f_2 and f_1-f_3 subspaces, we can see that the hypervolume contributions of solutions on the sides of the triangular Pareto front increase as the distance of the reference point from the Pareto front increases. On the contrary, the hypervolume contributions of solutions inside the triangular Pareto front do not increase (when they are dominated solutions in all two-dimensional subspaces). These discussions explain why all solutions are obtained on the sides of the triangular Pareto front in Figure 3 (b) when the reference point is far from the Pareto front.

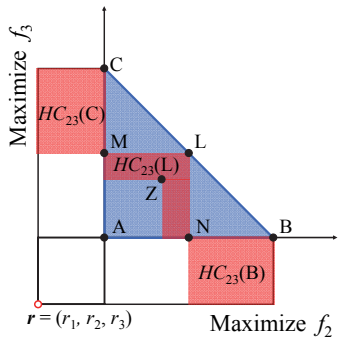

Figure 20. Projection of the Pareto front and the seven solutions to the two-dimensional subspace with f_2 and f_3. Hypervolume contribution of each solution in the subspace is shown by the shaded region in red.

These discussions can be generalized to the case of m objectives. For simplicity of explanation, we specify the reference point $\boldsymbol{r}$ as $\boldsymbol{r} = (r_1, r_2, ..., r_m) = (-r, -r, ..., -r)$ using a positive value r. Let us examine the projection of the triangular Pareto front (which is defined by $f_1 + f_2 + ... + f_m = 1$ and $0 \le f_i \le 1$ for $i = 1, 2, ..., m$ in the m-dimensional objective space) to its subspaces.

First we consider the projection of the Pareto front to the $(m-1)$-dimensional subspace with $f_2, f_3, ..., f_m$. The projected Pareto front can be written as $f_2 + ... + f_m \le 1$ and $0 \le f_i \le 1$ for $i = 2, ..., m$ (e.g., the projected Pareto front in Figure 20 is written as $f_2 + f_3 \le 1$ and $0 \le f_i \le 1$ for $i = 2, 3$). The set of the non-dominated solutions in the f_2-f_3- ... -f_m subspace can be written as $f_2 + ... + f_m = 1$ and $0 \le f_i \le 1$ for $i = 2, 3, ..., m$ (e.g., the set of the non-dominated solutions in Figure 20 is written as $f_2 + f_3 = 1$ and $0 \le f_i \le 1$ for $i = 2, 3$). The hypervolume contribution of each non-dominated solution in the f_2-f_3- ... -f_m subspace increases as the value of r_1 decreases (i.e., as the value of r increases). That is, their hypervolume contributions increase with r.

Next, let us consider the projection to the f_3-f_4- ... -f_m subspace. The projected Pareto front can be written as $f_3 + ... + f_m \le 1$ and $0 \le f_i \le 1$ for $i = 3, 4, ..., m$. The set of the non-dominated solutions in the f_3-f_4- ... -f_m subspace can be written as $f_3 + ... + f_m = 1$ and $0 \le f_i \le 1$ for $i = 3, 4, ..., m$. The hypervolume contribution of each non-dominated solution in the f_3-f_4- ... -f_m subspace increases as the values of r_1 and r_2 decrease (i.e., as the value of r increases). That is, their hypervolume contributions increase with r^2.

In the same manner, we can examine the projection of the m-dimensional objective space to its k-dimensional subspace. As the extreme case, let us examine the case with $k = 1$. The Pareto front in the m-dimensional objective space is projected to the interval [0, 1] in the single-dimensional subspace with f_m. The single point with $f_m = 1$ is the non-dominated solution in the interval [0, 1]. This point is the projection of the extreme solution (0, 0, ..., 0, 1). Its hypervolume contribution increases with r^{m-1} by increasing the value of r (i.e., by specifying the reference point far away from the Pareto front). This discussion holds for all extreme solutions. Thus, when the reference point is far from the Pareto front, the extreme solutions are likely to be in the optimal solution set. However, this is not always the case (e.g., when the number of solutions in the solution set is one, the Pareto optimal solution at the center of the Pareto front is the optimal selection).

When the triangular Pareto front in the m-dimensional objective space is projected to the 2-dimensional subspace with f_2 and f_3, the projected Pareto front is written as $f_2 + f_3 \le 1$ and $0 \le f_i \le 1$ for $i = 2, 3$ (see Figure 20). The set of the non-dominated solutions in the f_2-f_3 subspace is written as $f_2 + f_3 = 1$ and $0 \le f_i \le 1$ for $i = 2, 3$. The Pareto optimal solutions on the line between the two extreme solutions (0, 1, 0, ..., 0) and (0, 0, 1, 0, ..., 0) are projected to the non-dominated solutions in the f_2-f_3 subspace. Their hypervolume contributions increase with r^{m-2} when we increase the value of r. These discussions hold for all pairs of two extreme solutions. That is, the hypervolume contributions of the Pareto optimal solutions on the lines between any two extreme solutions increase with r^{m-2}. As a result, when the reference point is far from the Pareto front and the size of a solution set is much larger than the number of the extreme solutions, it is likely that some solutions on the line between each pair of the extreme solutions (i.e., some solutions on each edge of the m-dimensional triangular Pareto front) are included in the optimal solution set. These discussions explain why all the obtained solutions in Figure 19 are on the lines of the four extreme solutions (including the four extreme solutions).

3.3 Optimal Solution Sets

From the discussions in Subsection 3.2, we can obtain the following property with respect to the hypervolume contribution of a Pareto optimal solution of an m-objective maximization problem when the reference point $\boldsymbol{r} = (-r, -r, ..., -r)$ moves far away from the Pareto front: The hypervolume contribution of a Pareto optimal solution increases with r^{m-k} when it is a non-overlapping non-dominated solution in at least one k-dimensional subspace and not a non-overlapping non-dominated solution in any $(k-1)$-dimensional subspace. The condition "non-overlapping" is needed since overlapping solutions have no hypervolume contribution. This property also holds for an m-dimensional minimization problem with the reference point $\boldsymbol{r} = (r, r, ..., r)$.

Let us discuss the implication of this property for the case of $m = 3$ (i.e., three-objective problems) and a large value of r. In this case, Pareto optimal solutions in a solution set of a three-objective problem can be categorized into the following three classes:

Class 0: A Class 0 solution has no two-dimensional subspace where it is a non-overlapping non-dominated solution. Its hypervolume contribution does not increase when we increase the value of r.

Class 1: A Class 1 solution has at least one two-dimensional subspace and no single-dimensional subspace where it is a non-overlapping non-dominated solution. Its hypervolume contribution increases with r when we increase the value of r.

Class 2: A Class 2 solution has at least one single-dimensional subspace where it is a non-overlapping non-dominated solution. Its hypervolume contribution increases with r^2 when we increase the value of r.

For example, the Pareto optimal solutions of the normalized three-objective DTLZ1 problem in Subsection 3.1 are categorized as

(i) The three extreme solutions A (1, 0, 0), B (0, 1, 0), C (0, 0, 1):
If the three extreme solutions A, B and C are included in a solution set, they are Class 1 solutions. They are not Class 2 solutions because two of them always overlap at the point of $f_i = 0$ in each single-dimensional subspace.

(ii) All the other Pareto optimal solutions:
They are Class 0 solutions (when the three extreme solutions are included in the solution set). They are not Class 1 solutions because they are always dominated by one of the three extreme solutions in all of the two-dimensional subspaces (e.g., they are dominated by C (0, 0, 1) in the two-dimensional f_1-f_2 subspace).

When r is large, all the three extreme solutions are likely to be included in the optimal solution set. Let us consider a solution set S with μ ($\mu \geq 3$) solutions including two extreme solutions of the three-objective DTLZ1 problem. By adding the other extreme solution, we generate a new solution set S' with ($\mu + 1$) solutions including all the three extreme solutions. Then we generate a new solution set S'' by removing a single solution with the smallest hypervolume contribution from S'. Since the hypervolume contribution of each extreme solution increases with r and that of any other solution does not increase, we can specify a large value of r so that a non-extreme solution has the smallest hypervolume contribution. The obtained solution set S'' by removing such a non-extreme solution has a larger hypervolume than the solution set S for the specified value of r. This means that the solution set S excluding a single extreme solution cannot be the best solution set with μ ($\mu \geq 3$) solutions. Thus, we can say that all the three extreme solutions are included in the optimal solution set with μ ($\mu \geq 3$) solutions when r is large.

These discussions for the three-objective DTLZ1 problem can be generalized to the case of four or more objectives. That is, for the m-objective DTLZ1 problem, it is likely that all the m extreme solutions are included in the optimal solution set with μ ($\mu \geq m$) solutions. If a solution set includes all the m extreme solutions, the hypervolume contribution of any other solution does not increase when we increase the value of r.

Discussions for Max-DTLZ1 are more complicated. For example, the Pareto optimal solutions of the normalized three-objective Max-DTLZ1 problem in Subsection 3.2 are categorized as

(i) The three extreme solutions A (1, 0, 0), B (0, 1, 0), C (0, 0, 1):
If the three extreme solutions A, B and C are included in the solution set, they are Class 2 solutions. This is because each extreme solution is the non-overlapping best solution at $f_i = 1$ in the corresponding single-dimensional subspace with f_i.

(ii) All solutions on the sides of the Pareto front:
They are Class 1 solutions (if all the three extreme solutions are included in a solution set). As explained in Figure 20, each solution on a side of the Pareto front is a non-overlapping non-dominated solution in a two-dimensional subspace. They are not Class 2 solutions because their projections to each single-dimensional subspace with f_i are always dominated by an extreme solution at $f_i = 1$.

(iii) All the other Pareto optimal solutions:
If all the three extreme solutions and all solutions on the sides of the Pareto front are included in a solution set, all the other Pareto optimal solutions are Class 0 solutions. If solutions on a part of a side are not included in a solution set, some inside Pareto optimal solutions around the uncovered part can be Class 1 solutions. By increasing the number of solutions on the sides of the Pareto front, more inside solutions become Class 0 solutions.

When r is large (i.e., when the reference point is far from the Pareto front), all the three extreme solutions of the three-objective Max-DTLZ1 problem are likely to be included in the optimal solution set with μ solutions ($\mu \geq 3$). This can be explained in the same manner as the above discussions for the DTLZ1 problem. When r is large and $\mu > 3$, some Class 1 solutions are included in the optimal solution set. However, it is not likely that any Class 0 solution is included in the optimal solution set. Let us assume that a Class 0 solution is included in a solution set S with μ solutions. We generate a new solution set S' with (μ+1) solutions by adding a Class 1 solution. For the new solution set S', we can specify a large value of r so that the Class 0 solution has the smallest hypervolume contribution. A new solution set S'' is generated by removing the Class 0 solution with the smallest hypervolume contribution. Since S'' has a larger hypervolume than S, S is not the optimal solution set with μ solutions. That is, no Class 0 solution is included in the optimal solution set of the three-objective Max-DTLZ1 problem when r is large.

4. NEAR REFERENCE POINT

In this section, we discuss hypervolume maximization for the case where the reference point is the same as the nadir point or very close to the Pareto front (i.e., closer than the nadir point).

4.1 DTLZ1

First we discuss the case where the nadir point (1, 1, 1) of the normalized three-objective DTLZ1 problem is used as the reference point (see Figure 21). In this figure, it is clear that the hypervolume contribution of the three extreme solutions A, B and C is zero. Thus they are not included in the optimal solution set as shown in Figure 2 (a). However, solutions on the sides of the Pareto front have positive hypervolume contributions. Thus some solutions are obtained on the sides in Figure 2 (a).

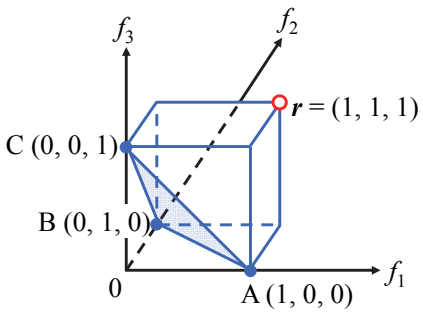

Figure 21. The normalized three-objective DTLZ1 Problem and the reference point (1, 1, 1).

For example, the hypervolume of solution M (0.5, 0, 0.5) at the midpoint between A and C is the volume of the following region:

$$D(\mathrm{M}, \boldsymbol{r}) = \{(z_1, z_2, z_3) \mid 0.5 \leq z_1 \leq 1,\ 0 \leq z_2 \leq 1,\ 0.5 \leq z_3 \leq 1\}. \quad (35)$$

Thus the hypervolume of M is 1/4, which is 1/4 of the volume of the unit cube $[0, 1]^3$. Whereas M has a large hypervolume, its contribution is decreased by other solutions. Let us consider the solution set {M, Z} where Z (1/3, 1/3, 1/3) is the solution at the center of the Pareto front. In this case, the hypervolume contribution of M is the volume of the following region:

$$\{(z_1, z_2, z_3) \mid 0.5 \leq z_1 \leq 1,\ 0 \leq z_2 \leq 1/3,\ 0.5 \leq z_3 \leq 1\}. \quad (36)$$

Thus the hypervolume contribution of M is calculated as 1/12. Let us consider another solution set {M, Y} where Y (0.25, 0, 0.75) is

a point on the line AC (see Figure 18). In this case, the hypervolume contribution of M is the volume of the region:

$$\{(z_1, z_2, z_3) \mid 0.5 \le z_1 \le 1,\ 0 \le z_2 \le 1,\ 0.5 \le z_3 \le 0.75\}. \quad (37)$$

Thus the hypervolume contribution is calculated as 1/8. As shown by these calculations, all Pareto optimal solutions except for the three extreme solutions have positive hypervolume contributions. The hypervolume contribution of a solution on the sides of the triangular Pareto front (and also a solution inside the Pareto front) is decreased by adding other solutions to the solution set. Since the hypervolume contribution of each solution is calculated in the unit cube $[0, 1]^3$, there exists no particular region (e.g., the sides of the triangular Pareto front) where solutions have dominatingly large hypervolume contributions. Thus solutions do not concentrate on a particular region of the Pareto front.

Next let us consider the case where the reference point is close to the Pareto front (more specifically, the reference point dominates the nadir point). For example, let us assume that the reference point is (0.6, 0.6, 0.6) in the normalized objective space with the nadir point (1, 1, 1) and the ideal point (0, 0, 0). Under this setting of the reference point, the hypervolume contribution is zero in the following part of the Pareto front: $0.6 \le f_1$, $0.6 \le f_2$ or $0.6 \le f_3$. This is because any solutions satisfying $0.6 \le f_1$, $0.6 \le f_2$ or $0.6 \le f_3$ do not dominate the reference point. Only solutions on the Pareto front between the three lines $f_1 = 0.6$, $f_2 = 0.6$ and $f_3 = 0.6$ in Figure 22 have positive hypervolume contributions. Figure 22 shows the obtained solutions by SMS-EMOA with 1,000,000 generations for the normalized three-objective DTLZ1 problem with the reference point (0.6, 0.6, 0.6). It should be noted that the hypervolume contribution of any solution on the three lines in Figure 22 is zero. So no solutions are obtained on the three lines. When the reference point is the nadir point (1, 1, 1), the three lines move to the three extreme solutions. In this case, the hypervolume contribution of each extreme solution is zero whereas all the other Pareto optimal solutions have positive hypervolume contributions. When the reference point is (0.5, 0.5, 0.5), the three lines in Figure 22 form the inscribed inverted triangle in the Pareto front. In Figure 4 (a), the reference point is specified as (0.5, 0.5, 0.5) in the normalized objective space. The obtained solutions are inside the inscribed inverted triangle in the Pareto front in Figure 4 (a).

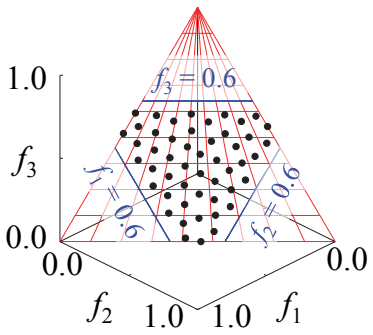

Figure 22. The obtained solutions by SMS-EMOA for the three-objective normalized DTLZ1 problem for the reference point (0.6, 0.6, 0.6).

Almost all discussions in this subsection can be extended to the case of four or more objectives. For example, when the nadir point is used as the reference point, no extreme solution of the triangular Pareto front on the hyperplane $f_1 + f_2 + \ldots + f_m = 1$ has a positive hypervolume contribution. Thus they are not included in the optimal solution set for hypervolume maximization. However, solutions on the sides of the Pareto front can be included in the optimal solution sets. When the reference point is close to the Pareto front (i.e., the reference point dominates the nadir point), solutions in the optimal solution set are inside an inverted triangular region of the Pareto front since no solutions outside the region have positive hypervolume contributions.

4.2 Max-DTLZ1 and Inverted DTLZ1

First we consider the case where the nadir point (0, 0, 0) is used as the reference point in the normalized three-objective Max-DTLZ1 problem. In this case, it is clear that the hypervolume contribution of all solutions on the sides of the triangular Pareto front is zero. For example, all solutions on the side between A (1, 0, 0) and C (0, 0, 1) in Figure 21 have zero as the value of the second objective. Thus the hypervolume contributions of all points on this line are always zero. As a result, no solutions are obtained on the sides of the triangular Pareto front as shown in Figure 3 (a).

Next let us consider the case where the reference point is very close to the Pareto front (i.e., the reference point dominates the nadir point). For example, let us assume that the reference point is (0.2, 0.2, 0.2) in the normalized objective space with the nadir point (0, 0, 0) and the ideal point (1, 1, 1). Under this setting, only Pareto optimal solutions inside the triangular region satisfying the following condition have positive hypervolume values: $0.2 \le f_1$, $0.2 \le f_2$ and $0.2 \le f_3$. This triangular region is shown in Figure 23 together with the obtained solutions by SMS-EMOA. Since no solutions on the sides of this triangular region have positive hypervolume contributions, no solutions are obtained on the sides of the smaller triangle in Figure 23. It is interesting to observe that solutions are obtained in the triangular region for Max-DTLZ1 (whereas they are obtained in the inverted triangular region for DTLZ1) when the reference point is close to the Pareto front. This observation may be a useful insight when we try to focus the search of an indicator-based algorithm on a small region of the Pareto front using a reference point. When the nadir point (0, 0, 0) is used as the reference point, the small triangle in Figure 23 becomes the same as the triangular Pareto front (see Figure 3 (a)).

Almost all discussions in this subsection can be extended to the case of four or more objectives. For example, when the nadir point (0, 0, ..., 0) is used as the reference point, no solutions on the sides of the triangular Pareto front are obtained in the optimal solution set of Max-DTLZ1 with four or more objectives. We may be able to focus on a small triangular region of the Pareto front by using a reference point close to the Pareto front.

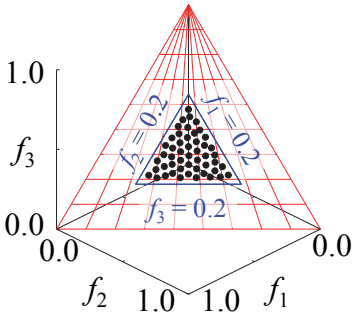

Figure 23. The obtained solutions by SMS-EMOA for the three-objective normalized Max-DTLZ1 problem for the reference point (0.2, 0.2, 0.2).

5. EFFECTS ON COMPARISON RESULTS

In this section, we examine the effect of the location of the reference point for hypervolume calculation on hypervolume-based performance comparison results of multiple solution sets. First we generated four solution sets by applying MOEA/D-PBI to the normalized three-objective DTLZ1 using four settings of the reference point in the PBI function: (0.2, 0.2, 0.2), (0.1, 0.1, 0.1), (0, 0, 0) and (−0.1, −0.1, −0.1). In the PBI function, we used only the distance d_2 from the reference line since all feasible solutions were Pareto optimal under our setting of the number of distance variables (i.e., $k = 0$). The population size was specified as 105. The generated solution sets are referred to as solution sets A, B, C and D as shown in Figure 24. For comparison, we also generated solution set E by uniformly sampling solutions only on the sides of the Pareto front. This solution set is shown in Figure 25.

Then we compared the five solution sets using the hypervolume where five settings of the reference point for hypervolume calculation were examined: (1.0, 1.0, 1.0), (1.1, 1.1, 1.1), (1.2, 1.2, 1.2), (1.5, 1.5, 1.5) and (2.0, 2.0, 2.0). The evaluation result of each solution set is shown as the rank among the five solution sets in Table 1 (1: the best, 5: the worst). Independent of the setting of the reference point for hypervolume calculation, we obtained the same performance comparison results for the five solution sets in Table 1. This observation is consistent with the discussions in Subsection 3.1 where we showed that the optimal distribution of solutions is independent of the reference point as long as the three extreme solutions are included in the solution set and the reference point is dominated by the nadir point.

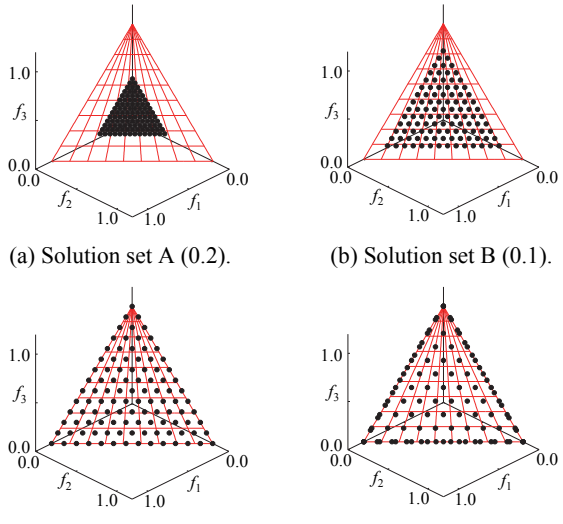

(a) Solution set A (0.2). (b) Solution set B (0.1).

(c) Solution set C (0.0). (d) Solution set D (−0.1).

Figure 24. Four solution sets obtained by MOEA/D-PBI.

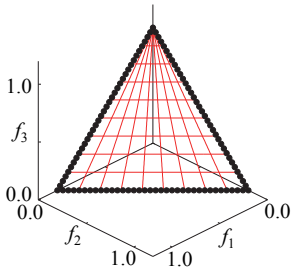

Figure 25. Solution set E.

Table 1. Ranking of the five solution sets when they are compared as solution sets of the normalized three-objective DTLZ1 Problem for each setting of the reference point: Comparison results for the minimization problem.

Reference Point	1.0	1.1	1.2	1.5	2.0
Solution set A	5	5	5	5	5
Solution set B	4	4	4	4	4
Solution set C	1	1	1	1	1
Solution set D	2	2	2	2	2
Solution set E	3	3	3	3	3

We also compared the five solution sets as solution sets of the normalized three-objective Max-DTLZ1 problem. Experimental results are shown in Table 2. When the nadir point (0, 0, 0) is used as the reference point, the solution set B has the largest hypervolume value. This may be because all solutions on the sides of the triangular Pareto front have no hypervolume contribution in this setting. When the reference point is a little bit smaller than the nadir point (i.e., (−0.1, −0.1, −0.1): a little bit away from the Pareto front than the nadir point (0, 0, 0)), the solution set C has the largest hypervolume value. When the reference point is far from the Pareto front (i.e., (−20, −20, −20)), the solution set E has the largest hypervolume value in Table 2. As shown in Table 2, performance comparison results depend heavily on the location of the reference point for hypervolume calculation.

Table 2. Ranking of the five solution sets when they are compared as solution sets of the normalized three-objective Max-DTLZ1 Problem for each setting of the reference point: Comparison results for the maximization problem.

Reference Point	0.0	−0.1	−0.2	−0.5	−20
Solution set A	4	4	5	5	5
Solution set B	1	3	3	4	4
Solution set C	2	1	1	2	3
Solution set D	3	2	2	1	2
Solution set E	5	5	4	3	1

Our experimental results on DTLZ1 (Table 1) and Max-DTLZ1 (Table 2) are consistent with our discussions on the optimal distribution of solutions in Section 3 and Section 4. We also performed computational experiments for the case of four objectives in the same manner as in Table 1 and Table 2. First MOEA/D-PBI with the population size 969 was applied to the normalized four-objective DTLZ1 problem to obtain four solution sets using four settings of the reference point: (0.2, 0.2, 0.2, 0.2), (0.1, 0.1, 0.1, 0.1), (0, 0, 0, 0) and (−0.1, −0.1, −0.1, −0.1). The obtained four solution sets are referred to as solution sets A, B, C and D, respectively. Solution set E with 969 solutions was generated by uniformly sampling solutions on the sides of the triangular Pareto front (i.e., solutions were sampled uniformly on the lines between all pairs of the four extreme solutions (1, 0, 0, 0), (0, 1, 0, 0), (0, 0, 1. 0) and (0, 0, 0, 1)). Then the five solution sets were compared using the hypervolume for different settings of the reference point for hypervolume calculation.

Table 3 shows the performance comparison results when the five solution sets were evaluated as solution sets of the normalized four-objective DTLZ1 problem. As in Table 1, we obtained the same performance comparison results independent of the setting of the reference point for hypervolume calculation in Table 3.

Table 3. Ranking of the five solution sets when they are compared as solution sets of the normalized four-objective DTLZ1 Problem for each setting of the reference point: Comparison results for the minimization problem.

Reference Point	1.0	1.1	1.2	1.5	2.0
Solution set A	5	5	5	5	5
Solution set B	4	4	4	4	4
Solution set C	1	1	1	1	1
Solution set D	2	2	2	2	2
Solution set E	3	3	3	3	3

We also compared the same five solution sets for the normalized four-objective Max-DTLZ1 problem. Experimental results are shown in Table 4. As in Table 2, the performance comparison results of the five solution sets in Table 4 heavily depend on the setting of the reference point for hypervolume calculation. For example, a different solution set is evaluated as being the best for each of the three similar specifications: 0.0, −0.1 and −0.2.

Table 4. Ranking of the five solution sets when they are compared as solution sets of the normalized four-objective Max-DTLZ1 Problem for each setting of the reference point: Comparison results for the maximization problem.

Reference Point	0.0	−0.1	−0.2	−0.5	−20
Solution set A	4	4	5	5	5
Solution set B	1	3	3	4	4
Solution set C	2	1	2	2	3
Solution set D	3	2	1	1	2
Solution set E	5	5	4	3	1

6. FURTHER EXAMINATIONS

In this section, we examine the property derived in Section 3: The hypervolume contribution of a Pareto optimal solution of an m-objective problem increases with r^{m-k} when it is a non-overlapping non-dominated solution in a k-dimensional subspace and not in any $(k-1)$-dimensional subspace. When it is not a non-overlapping non-dominated solution in any $(m-1)$-dimensional subspace, its hypervolume contribution does not increase with r.

6.1 DTLZ1 with a Constraint on f_3

We added a constraint condition $f_3(\boldsymbol{x}) \le 0.5$ to the three-objective normalized DTLZ1 problem. Its Pareto front is shown in Figure 26. All solutions on the line with $f_3(\boldsymbol{x}) = 0.5$ (i.e., all solutions on the line ML in Figure 26) are non-overlapping non-dominated solutions in the f_1-f_2 subspace. Computational experiments were performed using SMS-EMOA in the same manner as in Section 1. That is, the objective space was normalized for the original DTLZ1 problem without the constraint condition $f_3(\boldsymbol{x}) \le 0.5$ as shown in Figure 26.

Experimental results are shown in Figure 27 where we can observe a clear dependence of the obtained solution sets on the location of a reference point $\boldsymbol{r} = (r, r, r)$. This is because all Pareto optimal solutions on the line ML with $f_3(\boldsymbol{x}) = 0.5$ are non-overlapping non-dominated solutions in the f_1-f_2 subspace of the modified DTLZ1 problem in this subsection. By increasing the value of r (i.e., by moving the reference point far from the Pareto front), more solutions are obtained on the line ML (most solutions are on the line ML when $r = 100$).

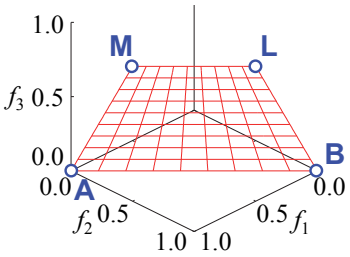

Figure 26. Pareto front of DTLZ1 with $f_3(\boldsymbol{x}) \le 0.5$.

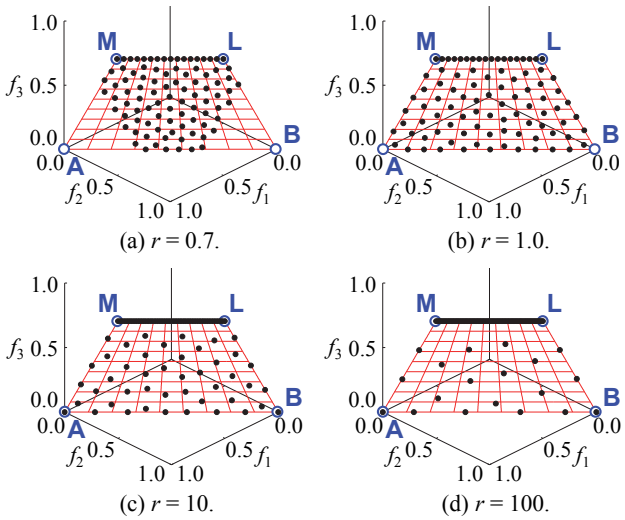

Figure 27. Obtained solution sets by SMS-EMOA for different reference points (DTLZ1 with $f_3(\boldsymbol{x}) \le 0.5$).

6.2 Inverted DTLZ1 with a Constraint on f_3

We added a constraint condition $f_3(\boldsymbol{x}) \ge 0.5$ to the three-objective normalized inverted DTLZ1 problem. Its Pareto front is shown in Figure 28. No Pareto optimal solution on the line ML with $f_3(\boldsymbol{x}) = 0.5$ except for M and L is non-dominated in any two-dimensional subspace (whereas all Pareto optimal solutions on the other sides of the Pareto front are non-overlapping non-dominated solutions in a two-dimensional subspace). Experimental results of SMS-EMOA are shown in Figure 29.

From Figure 29 (and also from Figure 27), we can see that many solutions were obtained on some sides of the Pareto front where the Pareto optimal solutions were non-overlapping non-dominated solutions in a two-dimensional subspace. More solutions were obtained on those sides by increasing the value of r (i.e., by moving the reference point far away from the Pareto front).

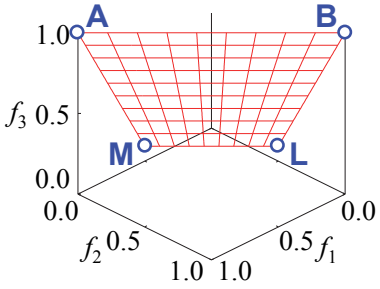

Figure 28. Pareto front of Inverted DTLZ1 with $f_3(\boldsymbol{x}) \ge 0.5$.

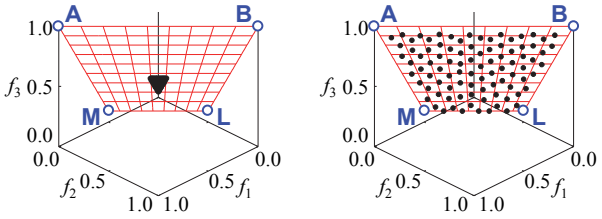

(a) $r = 0.7$. (b) $r = 1.0$.

(c) $r = 10$. (d) $r = 100$.

Figure 29. Obtained solution sets by SMS-EMOA for different reference points (Inverted DTLZ1 with $f_3(x) \geq 0.5$).

6.3 DTLZ1 with Constraints on f_1 and f_2

We added constraint conditions $f_1(x) \leq 0.5$ and $f_2(x) \leq 0.5$ to the three-objective normalized DTLZ1 problem. The Pareto front of this problem is shown in Figure 30. The projections of the Pareto front to the f_1-f_2, f_1-f_3 and f_2-f_3 subspaces are shown in Figure 31. In Figure 31 (a), only a single solution C is Pareto optimal in the f_1-f_2 subspace as in the three-objective normalized DTLZ1 problem. However, in Figure 31 (b), all Pareto optimal solutions on the line with $f_2(x) = 0.5$ (i.e., all Pareto optimal solutions on the line LN) are non-overlapping non-dominated solutions in the f_1-f_3 subspace. In Figure 31 (c), all Pareto optimal solutions on the line MN with $f_1(x) = 0.5$ are non-overlapping non-dominated solutions in the f_2-f_3 subspace. Experimental results of SMS-EMOA are shown in Figure 32. We can see from Figure 32 that many solutions were obtained on the lines LN and MN. By increasing the value of r, more solutions were obtained on the two lines.

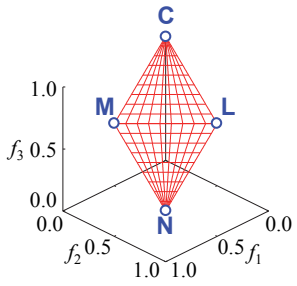

Figure 30. Pareto front of DTLZ1 with $f_1(x) \geq 0.5$ and $f_2(x) \geq 0.5$.

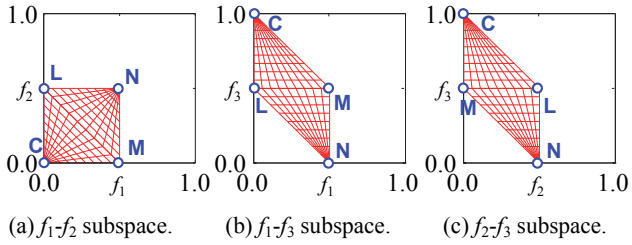

(a) f_1-f_2 subspace. (b) f_1-f_3 subspace. (c) f_2-f_3 subspace.

Figure 31. Projections of the Pareto front in Figure 30 to the two-dimensional subspaces.

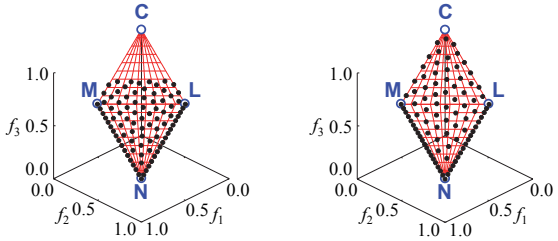

(a) $r = 0.7$. (b) $r = 1.0$.

(c) $r = 10$. (d) $r = 100$.

Figure 32. Obtained solution sets by SMS-EMOA for different reference points (DTLZ1 with $f_1(x) \geq 0.5$ and $f_2(x) \geq 0.5$).

6.4 WFG3

The WFG3 problem [14] was intended to be a test problem with a degenerate Pareto front. However, recently it has been shown in [16] that the WFG3 problem with three or more objectives has a non-degenerate part of the Pareto front in addition to the intended degenerate Pareto front. The Pareto front of the three-objective WFG3 test problem is shown in Figure 33. Its projections to the two-objective subspaces are shown in Figure 34. The line AB in Figure 33 is the originally intended degenerate Pareto front. Figure 34 shows that all solutions on the line AB in (b) and the line CB in (c) are non-overlapping non-dominated solutions in at least one of the three two-dimensional subspaces. In Figure 34 (a), solution A is the best solution (no other non-dominated solutions).

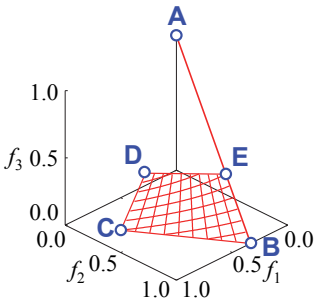

Figure 33. Pareto front of the three-objective WFG3 problem.

(a) f_1-f_2 subspace. (b) f_1-f_3 subspace. (c) f_2-f_3 subspace.

Figure 34. Projections of the Pareto front in Figure 33 to the two-dimensional subspace (WFG3).

Experimental results by SMS-EMOA are shown in Figure 35. We can see from Figure 35 that (almost) all solutions were obtained on the right and bottom boundaries of the Pareto front (i.e., on the lines AB and BC) when the reference point was far from the Pareto front. We can also see from Figure 35 that many solutions were not obtained inside the Pareto front even when $r = 1.0$ (i.e., even when the reference point was (1, 1, 1)). This is because all inside solutions have very small hypervolume contributions. We can also see that more solutions were obtained on an upper part of the line AB with large values of f_3 than its lower part with small values of f_3. This is because the upper part of AB is non-dominated in both the f_2-f_3 and f_1-f_3 subspaces whereas the lower part is non-dominated only in the f_2-f_3 subspace (see Figure 34).

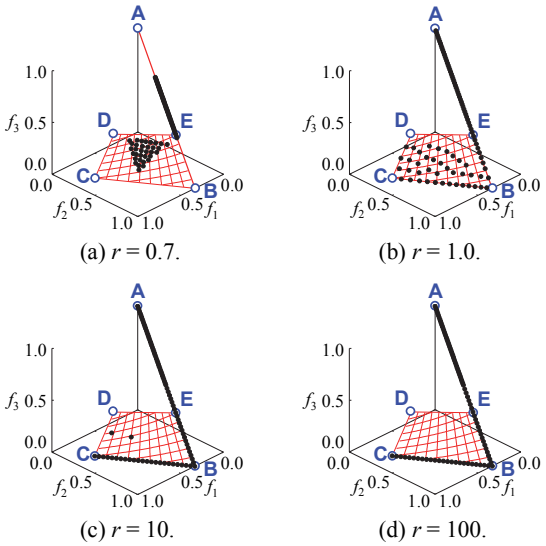

(a) $r = 0.7$. (b) $r = 1.0$.

(c) $r = 10$. (d) $r = 100$.

Figure 35. Obtained solution sets by SMS-EMOA (WFG3).

7. CONCLUDING REMARKS

In this paper, we discussed the optimal distribution of solutions for hypervolume maximization on the triangular Pareto fronts of the three-objective DTLZ1 test problem [8] and its two variants: inverted DTLZ1 [19] and Max-DTLZ1 [18]. Our contribution was to show that the optimal distribution is totally different between three-objective minimization and maximization problems even when they have the same triangular Pareto front. This fact has not necessarily been well recognized in the EMO community because such a large difference does not exist in the case of two objectives. This is also because maximization problems with triangular Pareto fronts and minimization problems with inverted triangular Pareto front have not been used in many studies.

The reason for the large difference in the optimal distribution of solutions between three-objective minimization and maximization problems is that the extreme solutions play different roles. In the case of a three-objective minimization problem with a triangular Pareto front, the optimal distribution of solutions can be discussed within the unit cube $[0, 1]^3$ in the normalized objective space independent of the location of the reference point (when the three extreme solutions are included in a solution set and the reference point is far from the Pareto front). This is because the outside of the unit cube $[0, 1]^3$ is dominated by at least one extreme solution. As a result, a set of the three extreme solutions and well-distributed solutions over the entire Pareto front has a large hypervolume value independent of the location of the reference point for hypervolume calculation as far as the reference point is far from the Pareto front. However, in the case of a three-objective maximization problem with a triangular Pareto front, the optimal distribution of solutions heavily depends on the location of the reference point. For example, when the reference point is far from the Pareto front, a larger hypervolume value is obtained from a set of solutions on the sides of the Pareto front than a set of well-distributed solutions over the entire Pareto front. This is because the extreme solutions cannot dominate all the regions outside the unit cube $[0, 1]^3$. As a result, every solution on each side of the triangular Pareto front is non-dominated on the corresponding two-dimensional subspace of the three-dimensional objective space. Thus their hypervolume contributions increase as the reference point moves away from the Pareto front.

From our discussions in this paper, one may think that minimization problems with triangular Pareto fronts such as DTLZ1 seem to have a good property as test problems in their performance evaluation: robustness with respect to the location of the reference point. We do not have to examine multiple reference points for hypervolume calculation, which leads to multi-objective solution set optimization [15]. However, minimization problems with triangular Pareto fronts have a somewhat strange property as multiobjective test problems: A single extreme solution of an m-objective problem simultaneously optimizes $(m-1)$ objectives. For example, an extreme solution (1, 0, 0, 0) simultaneously optimizes the second, third and fourth objectives of a four-objective minimization problem with the normalized triangular Pareto front where the ideal point is (0, 0, 0, 0) and the nadir point is (1, 1, 1, 1). If we remove the first objective to formulate a three-objective problem, the formulated three-objective problem has a single optimal solution for all objectives. This strange property is related to the robustness of minimization problems with triangular Pareto fronts with respect to the location of the reference point in hypervolume-based performance comparison results.

On the contrary, performance comparison results of solution sets of maximization problems with triangular Pareto fronts strongly depend on the location of the reference point for hypervolume calculation. In our computational experiments on the three-objective and four-objective Max-DTLZ1 problems, a different solution set had the largest hypervolume for a different reference point. Our experimental results suggest that we should be careful when performance is compared for multiobjective maximization problems with triangular Pareto fronts (and many other test problems with constraint conditions as shown in Section 6). For those test problems, multiple reference points may be needed [15]. Whereas maximization problems with triangular Pareto fronts (i.e., minimization problems with inverted triangular Pareto fronts) do not have robustness with respect to the location of the reference point in hypervolume-based performance comparison, their extreme points do not have the above-mentioned strange property. Each extreme solution optimizes only a single objective. For example, the extreme solution (1, 0, 0, 0) optimizes only the first objective of a four-objective maximization problem while it simultaneously optimizes all the other three objectives of a four-objective minimization problem with a triangular Pareto front.

Whereas we clearly demonstrated the difference in the effect of the reference point on the optimal distribution of solutions between three-objective minimization and maximization problems, we did not theoretically derive any optimal distribution of solutions in a three-dimensional objective space. Derivation of the optimal distributions of solutions for triangular and inverted triangular Pareto fronts is left for future research.

8. REFERENCES

[1] Auger, A., Bader, J., Brockhoff, D., and Zitzler, E. 2009. Theory of the hypervolume indicator: Optimal μ-distributions and the choice of the reference point. In *Proceeding of 10th International Workshop on Foundations of Genetic Algorithms* (Orlando, USA, January 9-11, 2009) 87-102. DOI: http://doi.acm.org/10.1145/1527125.1527138

[2] Auger, A., Bader, J., Brockhoff, D., and Zitzler, E. 2012. Hypervolume-based multiobjective optimization: Theoretical foundations and practical implications. *Theoretical Computer Science* 425 (March 2012) 75-103.

[3] Bader, J. and Zitzler, E. 2011. HypE: An algorithm for fast hypervolume-based many-objective optimization. *Evolutionary Computation* 19, 1 (Spring 2011) 45-76.

[4] Basseur, M., Derbel, B., Goëffon, A., and Liefooghe, A. 2016. Experiments on greedy and local search heuristics for *d*-dimensional hypervolume subset selection. In *Proceedings of 2016 Genetic and Evolutionary Computation Conference* (Denver, USA, July 20-24, 2016) 541-548. DOI: http://doi.acm.org/10.1145/2908812.2908949

[5] Beume, N., Naujoks, B., and Emmerich, M. 2007. SMS-EMOA: Multiobjective selection based on dominated hypervolume. *European Journal of Operational Research* 180, 3 (September 2007) 1653-1669.

[6] Bringmann, K., Friedrich, T., and Klitzke, P. 2014. Generic postprocessing via subset selection for hypervolume and epsilon-indicator. *Lecture Notes in Computer Science 8672: Parallel Problem Solving from Nature - PPSN XIII* (Ljubljana, Slovenia, September 13-17, 2014) 518–527.

[7] Bringmann, K., Friedrich, T., and Klitzke, P. 2014. Two-dimensional subset selection for hypervolume and epsilon-indicator. In *Proceedings of 2014 Genetic and Evolutionary Computation Conference* (Vancouver, Canada, July 12-16, 2014) 589-596. DOI: http://doi.acm.org/10.1145/2576768.2598276.

[8] Deb, K., Thiele, L., Laumanns, M., and Zitzler, E. 2002. Scalable multi-objective optimization test problems. In *Proceedings of 2002 Congress on Evolutionary Computation* (Honolulu, USA, May 12-17, 2002) 825-830.

[9] Emmerich, M. T. M., Deutz, A. H., and Beume, N. 2007. Gradient-based/evolutionary relay hybrid for computing Pareto front approximations maximizing the S-metric. *Lecture Notes in Computer Science 4771: Hybrid Metaheuristics - HM 2007* (Dortmund, Germany, October 8-9, 2007) 140-156.

[10] Friedrich, T., Neumann, F., and Thyssen, C. 2015. Multiplicative approximations, optimal hypervolume distributions, and the choice of the reference point. *Evolutionary Computation* 23, 1 (Spring 2015) 131-159.

[11] Glasmachers, T. 2014. Optimized approximation sets for low-dimensional benchmark Pareto fronts. *Lecture Notes in Computer Science 8672: Parallel Problem Solving from Nature - PPSN XIII*. (Ljubljana, Slovenia, September 13-17, 2014) 569-578.

[12] Guerreiro, A. P., Fonseca, C. M., and Paquete, L. 2015. Greedy hypervolume subset selection in the three-objective case. In *Proceedings of 2015 Genetic and Evolutionary Computation Conference.* (Madrid, Spain, July 11-15, 2015) 671-678. DOI: http://doi.acm.org/10.1145/2739480.2754812

[13] Guerreiro, A. P., Fonseca, C. M., and Paquete, L. 2016. Greedy hypervolume subset selection in low dimensions. *Evolutionary Computation* 24, 3 (Fall 2016) 521-544.

[14] Huband, S., Hingston, P., Barone, L., and While, L. 2006. A review of multiobjective test problems and a scalable test problem toolkit. *IEEE Trans. on Evolutionary Computation* 10, 5 (October 2006) 477-506.

[15] Ishibuchi, H., Masuda, H., and Nojima, Y. 2014. Meta-level multi-objective formulations of set optimization for multi-objective optimization problems: Multi-reference point approach to hypervolume maximization, *Companion of 2014 Genetic and Evolutionary Computation Conference* (Vancouver, Canada, July 12-16, 2014) 89-90.

[16] Ishibuchi, H., Masuda, H., and Nojima, Y. 2016. Pareto fronts of many-objective degenerate test problems. *IEEE Trans. on Evolutionary Computation* 20, 5 (October 2016) 807-813.

[17] Ishibuchi, H., Setoguchi, Y., Masuda, H., and Nojima, Y. 2016. How to compare many-objective algorithms under different settings of population and archive sizes. In *Proceedings of 2016 IEEE Congress on Evolutionary Computation* (Vancouver, July 24-29, 2016) 1149-1156.

[18] Ishibuchi, H., Setoguchi, Y., Masuda, H., and Nojima, Y. 2016. Performance of decomposition-based many-objective algorithms strongly depends on Pareto front shapes. *IEEE Trans. on Evolutionary Computation* (Early Access). http://ieeexplore.ieee.org/xpl/tocresult.jsp?isnumber=4358751

[19] Jain, H. and Deb, K. 2014. An evolutionary many-objective optimization algorithm using reference-point based non-dominated sorting approach, Part II: Handling constraints and extending to an adaptive approach. *IEEE Trans. on Evolutionary Computation* 18, 4 (August 2014) 602-622.

[20] Kuhn, T., Fonseca, C. M., Paquete, L., Ruzika, S., Duarte, M. M., and Figueira, J. R. 2016. Hypervolume subset selection in two dimensions: Formulations and algorithms. *Evolutionary Computation* 24, 3 (Fall 2016) 411-425.

[21] Shukla, P.K., Doll, N., and Schmeck, H. 2014. A theoretical analysis of volume based Pareto front approximations. In *Proceedings of 2014 Genetic and Evolutionary Computation Conference* (Vancouver, Canada, July 12-16, 2014) 1415-1422. http://doi.acm.org/10.1145/2576768.2598348

[22] Zitzler, E., Brockhoff, D., and Thiele, L. 2007. The hypervolume indicator revisited: On the design of Pareto-compliant indicators via weighted integration. *Lecture Notes in Computer Science 4403: Evolutionary Multi-Criterion Optimization - EMO 2007* (Matsushima, Japan, March 5-8, 2007) 862-876.

[23] Zitzler, E. and Thiele, L. 1998. Multiobjective optimization using evolutionary algorithms - A comparative case study. *Lecture Notes in Computer Science 1498: Parallel Problem Solving from Nature - PPSN V* (Amsterdam, Netherlands, September 27-30) 292-301.

[24] Zitzler, E., Thiele, L., Laumanns, M., Fonseca, C.M., and da Fonseca, V.G. 2003. Performance assessment of multiobjective optimizers: An analysis and review. *IEEE Trans. on Evolutionary Computation* 7, 2 (April 2003) 117-132.